Nanoscale Horizons

ROYAL SOCIETY OF CHEMISTRY

COMMUNICATION

View Article Online
View Journal | View Issue

Check for updates

Cite this: *Nanoscale Horiz.*, 2025, **10**, 3376

Received 7th May 2025,
Accepted 8th September 2025

DOI: 10.1039/d5nh00317b

rsc.li/nanoscale-horizons

Transformative therapy in acute microbial-induced colitis with inflammation triggered micelles and combination therapies

Saman Ghazvini,[ab] Sepehr Hejazi,[a] Saji Uthaman, †[b] Tyler Harm,[c] Michael Wannemuehler[bc] and Rizia Bardhan *[ab]

Ulcerative colitis has no cure and there are limited options for patients. Many current therapeutic drugs have poor bioavailability and targeting ability, including inhibitors of the cGAS–STING pathway, which has limited their clinical approval for colitis. Here we address this critical need through inflammation-triggered nanomicelles (ITMs) that are composed of biopolymer hyaluronic acid which specifically targets the inflamed colon by binding to CD44 receptors. ITMs encapsulate the cGAS inhibitor RU.521 improving the drug's overall bioavailability, and utilize a reactive oxygen species (ROS)-responsive thioketal linker, enabling site-specific drug release at the inflamed colon. The efficacy of ITMs was shown in a clinically relevant microbial-induced colitis model that recapitulates human colitis. Acute colitis was developed in gnotobiotic altered Schaedler's flora (ASF) IL-10 knockout mice infected with *Helicobacter bilis* or *Escherichia coli* 1D to induce severe and moderate colitis, respectively. Oral delivery of ITMs alone significantly reduced inflammation in the *E. coli* 1D model, while combining ITMs with anti-IL-12p40 antibodies mitigated disease severity in the *H. bilis* model as revealed by body weight recovery, reduced colon shortening, restoration of the intestinal epithelium, and reduction in proinflammatory cytokines. *In vivo* end points were validated with *ex vivo* tissue imaging and assays that identified the downregulation of cGAS expression and other mechanisms by which ITMs enable mucosal healing. These findings highlight the potential of ITMs for targeted, site-specific drug delivery as a novel IBD treatment strategy, and the importance of inhibiting the cGAS–STING pathway in inflammatory diseases.

New concepts

Here we report innovative inflammation-triggered nanomicelles that are synthesized with hyaluronic acid (HA) and stearic acid biopolymers. These nanomicelles enable programmable drug delivery through a thioketal linker that is cleaved in the presence of reactive oxygen species (ROS) *in vivo*. We demonstrated dynamic drug release in the inflamed colon of mouse models of acute colitis which has high endogenous ROS arising from inflammation. The micelles also leverage the well-established molecular interactions between HA and CD44, where CD44 is a receptor overexpressed on the inflamed colonic mucosa and macrophages. Therefore, these micelles naturally target the inflamed colon without requiring further biochemical modification of the micellar surface. The innovation of this work also lies in the ability of the micelles to downregulate the cGAS–STING pathway with RU.521, a highly potent small molecule inhibitor but with poor bioavailability and targeting ability. The efficacy of the micelles was examined in a clinically relevant microbial model of colitis, *i.e.*, in gnotobiotic altered Schaedler's flora (ASF) IL-10 knockout mice infected with *Helicobacter bilis* or *Escherichia coli* 1D to simulate severe and moderate colitis, respectively. Oral delivery of micelles reduced inflammation in the *E. coli* 1D model, while combining micelles with anti-IL-12p40 antibodies mitigated disease severity in the *H. bilis* model.

1. Introduction

Ulcerative colitis is a chronic inflammatory disorder of the gastrointestinal (GI) tract that results in loss of intestinal barrier function and poor quality of life.[1] Colitis is also associated with dysbiosis of the gut microbiota, characterized by a reduction in microorganisms considered to be beneficial to the host.[2] Innate immunity is crucial for maintaining intestinal homeostasis and plays a significant role in the pathogenesis of inflammatory bowel diseases (IBDs).[3] Central to this process are innate receptors that regulate immune responses, including the cyclic GMP-AMP synthase-stimulator of interferon genes (cGAS–STING) pathway.[4,5] Recent studies in both mouse models of IBD[6] and IBD patients[7,8] have clearly demonstrated a significant upregulation of the cGAS–STING pathway. While the role of STING has been studied extensively in cancer,

[a] *Department of Chemical and Biological Engineering, Iowa State University, Ames, IA 50011, USA. E-mail: rbardhan@iastate.edu*
[b] *Nanovaccine Institute, Iowa State University, Ames, IA 50012, USA*
[c] *Department of Veterinary Microbiology and Preventive Medicine, Iowa State University, Ames, IA 50011, USA*
† Current address: Smart Materials and Devices (SMAD) Division, Yenepoya Research Centre, Yenepoya (Deemed to be University), Mangalore, 575018, India.

over-activation of STING has also been associated with other inflammatory diseases.[9,10] Despite these studies that underscore the importance of inhibition of cGAS as a target for the attenuation of colitis, there are no clinically approved cGAS-specific inhibitors available to treat IBDs. This is in part due to the low bioavailability after oral delivery, poor pharmacokinetics, and poor inflammation site targeting of these drugs which all contribute to systemic toxicity and debilitating side-effects.[11] Indeed, a number of small molecule inhibitors and biologicals are available for IBD treatment, but due to the aforementioned limitations, treatment efficacy has been subpar with poor long-term outcomes.[12]

Nanoformulations have transformed the landscape of drug delivery, enabling targeted and localized accumulation at the disease site, and recent studies have shown the efficacy of nanoformulations in IBDs.[13–16] However, many nanoformulations cannot withstand the harsh environment of the stomach, requiring systemic delivery that induces off-target toxicity, and would ultimately have an undue burden on patients, necessitating repeated hospital visits. In this work, inflammation-triggered nanomicelles (ITMs) were engineered with hyaluronic acid (HA) that allows targeted accumulation at the site of gut inflammation *via* the well-established binding of HA to CD44 receptors.[17] CD44 is upregulated on the surface of the colonic epithelium and pro-inflammatory macrophages.[18] ITMs also leverage a reactive oxygen species (ROS) responsive thioketal (TK) linker[19] that triggers micelle disruption and drug release in the presence of inflammation.[20,21] ROS is generated through the expression of inducible nitric oxide synthase (iNOS) upregulated in the inflamed gut. The TK functional group is cleaved into non-toxic thiol-containing molecules in the presence of ROS. ITMs are loaded with an inhibitor of the cGAS–STING pathway, RU.521, a drug that has been shown to downregulate cGAS-aggravated inflammatory responses *in vitro*[11] and *in vivo*,[22] and facilitate the restitution of the intestinal epithelium.[23] In our previous proof-of-concept study, we showed the efficacy of micelles in dextran sulfate sodium (DSS) induced colitis, a model widely employed in IBD research.[22] However, the DSS-induced colitis model does not replicate human colitis, and is therefore limited in studying how the gut microbiome contributes to the development of intestinal inflammation.[24] In this work, we demonstrate the efficacy of ITMs in the attenuation of inflammation *in vivo* in a clinically relevant microbial-induced colitis model that recapitulates human colitis more closely.

Here, gnotobiotic, altered Schaedler's flora (ASF) IL-10 knockout (KO) mice on a 129S6 background were used for the bacterial-induced colitis model. The ASF consists of a community of 8 known murine bacterial species (Table S1) representing a simplified microbiota that facilitates to study the functional changes in the gut microbiota following treatment.[25,26] The functional genetic content of the ASF when compared to wild-type murine metagenomes showed that ASF functionally represents and serves as an experimentally tractable surrogate for wild-type microbiomes.[27] The ASF model is clinically relevant because patients with IBDs are also known to have a dramatic reduction (*i.e.*, dysbiosis) in beneficial microorganisms including members of *Clostridium, Lactobacillus*, and *Eubacterium* that are present in the ASF (Table S1). These beneficial microorganisms promote gut health by promoting regulatory T cell (T_{reg}) functions. IL-10, an immunoregulatory cytokine with anti-inflammatory functions, regulates intestinal inflammation in both mouse models and humans, and IL-10 KO mice are a well-established model of acute and chronic colitis.[2,28] IL-10 KO mice also simulate the pre-disposed human patients who have polymorphisms in their IL-10 gene that makes them prone to colitis at an earlier age.[29,30] Here, we chose ASF IL-10 KO mice because when colonized with a pathobiont, these mice reproducibly develop bacterial-induced colitis in ~1–4 weeks relative to wild-type mice which require >4 months.[31]

In this work, ASF IL-10 KO mice were colonized with *Helicobacter bilis* (*H. bilis*) to induce severe acute colitis[32,33] and with *E. coli* 1D, a strain of attaching and invasive *E. coli* (AIEC) derived from a dog, to induce moderate colitis.[34] We particularly chose these two pathobionts to enable a broader spectrum of acute colitis severity that occurs in patients. Our findings show that in the *E. coli* 1D challenge model, RU.521-loaded ITMs alone were effective in ameliorating inflammation and protecting the mice from colon shortening. In the severe *H. bilis* model, the combination of ITMs with anti-IL-12p40 monoclonal antibodies (mAbs) was highly effective at attenuating bodyweight loss, reducing proinflammatory cytokines, alleviating colon injury, and reducing epithelial damage. Note that approximately 50% of IBD patients who initially respond to monotherapies with biologics or small molecules ultimately acquire resistance.[35] Therefore, advanced combination therapies are now being adopted in clinical practice[35,36] and have shown success in clinical trials (NCT03662542, NCT02764762). In both models, we found upregulation of cGAS expression in the untreated colitis group and successful downregulation with ITMs. Our findings highlight the transformative potential of ITMs and combination therapies in reducing intestinal inflammation, and the potential to ultimately allow a "functional cure" by promoting long-term protection against chronic colitis.

2. Results and discussion

2.1. Synthesis and characterization of the hyaluronic acid/stearic acid conjugate and ITMs

ITMs were synthesized by self-assembly of the HA and stearic acid (SA) conjugate, and triggered drug release was enabled through a TK linker. The conjugate, NH_2–TK–SA–HA, was synthesized through a series of reactions represented in Scheme S1 and reported in our previous work.[22] The TK linker with amine terminals was synthesized as previously described.[22] The amino groups of the synthesized TK linker were then reacted with the carboxylic group of stearic acid (SA), resulting in TK–SA, using carbodiimide coupling (EDC/NHS). The TK–SA conjugate was reacted with HA through a carbodiimide coupling reaction to synthesize the polymer that would subsequently self-assemble to form ITMs. The composition of ITMs was confirmed with proton

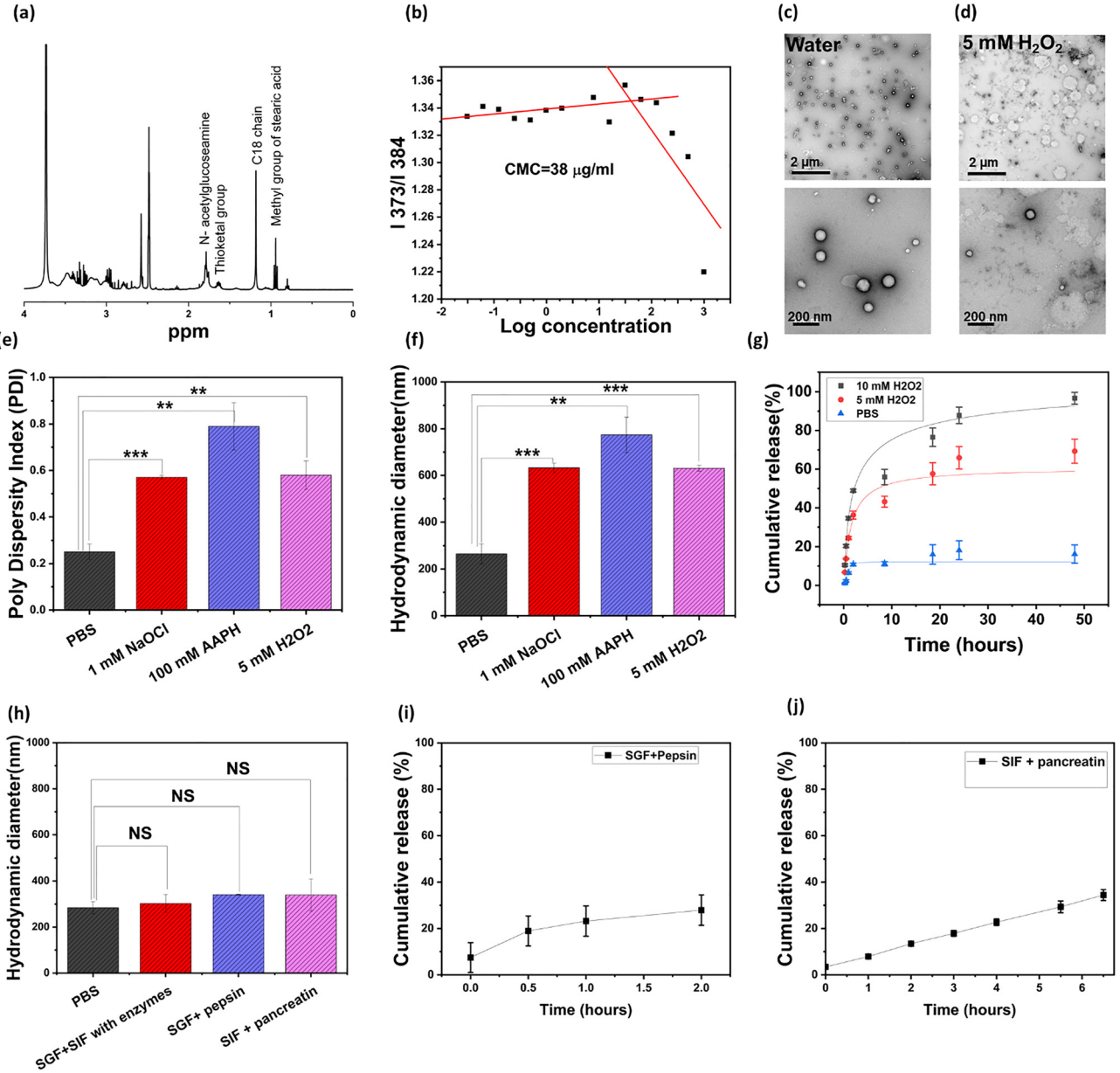

Fig. 1 Physicochemical properties of inflammation-triggered micelles (ITMs). (a) ^{1}H-NMR spectra of NH_2–TK–SA–HA in DMSO-D6 : D_2O. (b) Critical micellar concentration of ITMs. TEM images of RU.521 loaded micelles (c) incubated in DI water at two different magnifications (top: low magnification, bottom: high magnification) and (d) after incubating in 5 mM H_2O_2 showing ITMs' disintegration in presence of ROS. The scale bar is 2 μm for the low magnification images (top) and 200 nm for the high magnification images (bottom). (e) Polydispersity index (PDI) and (f) average hydrodynamic diameter of RU.521 loaded ITMs incubated in PBS and in solutions containing free radicals including 1 mM NaOCl, 100 mM AAPH, and 5 mM H_2O_2. (g) Cumulative drug release of RU.521 from ITMs in PBS *versus* 5 and 10 mM H_2O_2. (h) Average hydrodynamic diameter of RU.521 loaded micelles in PBS in comparison to micelles incubated in simulated gastric fluid with pepsin and simulated intestinal fluid with pancreatin. Cumulative drug release of RU.521 from ITMs in (i) simulated gastric fluid with pepsin and (j) simulated intestinal fluid with pancreatin. Experiments were run in triplicate and are presented as average ± standard deviation. Statistical significance is reported by a 2-tailed Student's *t*-test $*p < 0.05$, $**p < 0.01$, and $***p < 0.001$.

nuclear magnetic resonance (^{1}H-NMR) and FTIR analysis, which can be found in Fig. S1. The chemical shift δ (ppm) 1.17 shown in ^{1}H-NMR (Fig. 1(a)) corresponds to the methylene groups ($CH_2CH_2CH_2$), whereas δ (ppm) 0.94 refers to the terminal methyl groups (CH_3) of C18. The peak corresponding to the acetamido moiety (–$NHCOCH_3$) of the *N*-acetyl-D-glucosamine residue of HA was seen at δ (ppm) 1.78. In addition, the –$SC(CH_3)_2$ methyl groups in TK were observed as a chemical shift of δ (ppm) 1.63. The presence of these peaks confirms the successful conjugation of TK to HA and SA. The degree of substitution for stearic acid in the polymer was calculated to be 24% by dividing the integral of the peak corresponding to the terminal methyl group (δ 0.94 ppm) by the integral of the peak corresponding to *N*-acetylglucosamine (δ ppm 1.78), which means 24% of HA's carboxyl groups were substituted with the hydrophobic NH2-TK-SA group. The cGAS-inhibitor, RU.521, was loaded into the ITMs *via* sonication. The

critical micellar concentration (CMC) is useful in determining the lowest concentration of a polymer needed to generate micelles. Using pyrene as the fluorescent probe, the CMC was measured to be 38 μg ml^{-1} (Fig. 1(b)). ITMs' morphology was assessed with transmission electron micrographs (TEM, Fig. 1(c)) showing spherical micelles formed with an average size of 253 ± 88 nm. An average hydrodynamic diameter of 297.15 ± 8.45 nm and a polydispersity index (PDI) of ~0.2 were confirmed with DLS (Fig. 1(e) and (f)). The drug, RU.521, is encapsulated within ITMs' hydrophobic core, which is formed *via* the self-assembly of stearic acid, allowing the hydrophobic regions of the drug to interact with the hydrophobic chain of stearic acid. RU.521 loading content in ITMs was calculated to be 8.66 ± 0.93%. The free drug was removed *via* dialysis. The micelle solution was analyzed before and after dialysis, which showed a decrease in the characteristic peak of RU.521, confirming that the free drug was removed (Fig. S2). Throughout this study, RU.521 at 100 μM concentration was used as the dosage for *in vitro* and *in vivo* experiments. After ITMs are incubated in 5 mM hydrogen peroxide (hydroxyl radical generator), the micellar structure ruptures in the presence of free radicals, as represented in TEM photomicrographs (Fig. 1(d)) showing structural changes of the ITMs. The ROS-responsive degradation of ITMs was further confirmed by incubating ITMs with various ROS generators that include sodium hypochlorite (NaOCl, free radical generator), hydrogen peroxide (H_2O_2, hydroxyl radical generator), and 2,2-azobis(2-amidinopropane) dihydrochloride (AAPH, peroxy radical generator). The hydrodynamic size and PDI (Fig. 1(e) and (f)) of ITMs both increased relative to the samples dispersed in PBS indicating the successful dissociation of ITMs in response to ROS. Next, the drug release profile of RU.521 loaded in ITMs was evaluated in PBS with and without H_2O_2 to recapitulate the conditions of inflamed and healthy colon respectively. The significantly higher cumulative drug release from ITMs when incubated with both 5 mM and 10 mM H_2O_2 compared to PBS suggests that this ROS-responsive property of ITMs could be leveraged to target the inflamed colon *in vivo* (Fig. 1(g)). The stability of ITMs during oral delivery was further evaluated to assess their ability to withstand the harsh environment of the gastrointestinal tract. ITMs were incubated for 2 hours in simulated gastric fluid supplemented with pepsin, followed by a 6 hour incubation period in simulated intestinal fluid supplemented with pancreatin. Minimal changes were observed in the hydrodynamic diameter of ITMs when incubated with the simulated fluids (Fig. 1(h)) as well as minimal drug leakage (Fig. 1(i) and (j)) confirming that ITMs are stable in the gastrointestinal environment.

2.2. Therapeutic efficacy of ITMs *in vitro* in macrophages and epithelial cells

The uptake, targeting, and anti-inflammatory response of ITMs were studied *in vitro* in two different murine cell lines: J774.A1 macrophages and MODE-K epithelial cells. Our rationale for the choice of these cells was to assess if ITMs interacted with multiple resident cell types in the inflamed colon including macrophages and epithelial cells. The toxicity of 100 μM RU.521 loaded ITMs was studied *via* a CCK-8 assay. J774.A1 cells showed high viability when incubated with drug loaded ITMs at various concentrations (Fig. 2(a)). MODE-K cells were slightly more susceptible to toxicity at high concentrations of ITMs (50 μg ml^{-1}) but still had high viability at lower doses (Fig. 2(b)). To visualize intracellular uptake of ITMs, a near-infrared dye, IR780, was loaded in the micelles and then the IR780-loaded micelles were incubated with LPS-treated J774A.1 macrophages and MODE-K cells. To confirm active targeted delivery of micelles in the cells *via* CD44 receptors, which are overexpressed on both macrophages and epithelial cells following LPS stimulation, cells were pre-treated with HA to block the CD44 receptors.[37–39] The fluorescence (FL) images in both J774A.1 (Fig. 2(c)) and MODE-K (Fig. 2(d)) cells show minimal uptake of IR780-loaded micelles indicated by the lower Cy7 FL signal when CD44 receptors were blocked and an increase in the Cy7 signal without CD44 blocking. These findings confirm CD44-mediated active targeting and endocytosis of ITMs in both proinflammatory macrophages and inflamed epithelial cells (MODE-K). We next assessed if ITM treatment reduced the secretion of pro-inflammatory cytokines from LPS-treated J774.A1 (Fig. 2(e)–(h)) and MODE-K cells (Fig. 2(i)); free RU.521 at an equivalent dose (100 μM) was used as a positive control. In the LPS-treated J774.A1 cells, several pro-inflammatory cytokines including IL-1β, IL-12p40, IL-6 and TNF-α were significantly downregulated, while LPS-treated MODE-K cells only showed a decrease in secreted IL-6 levels with ITM treatment and other cytokines were below the detection limit of the Luminex platform (less than 3 pg ml^{-1}, data not shown). These findings suggest that (i) inflammation in intestinal epithelial cells (IECs) is less pronounced compared to that in macrophages in the context of colitis, and (ii) ITMs are more impactful in ameliorating inflammation in macrophages since a moderate concentration of ROS is needed for the micelles to trigger drug release. Further, NF-κB p65 was measured using a semi-quantitative ELISA kit (Abcam, ab176663) in the cell lysates of both J774A.1 and MODE-K cells since NF-κB is a major transcription factor regulating pro-inflammatory responses and is involved in the pathogenesis of colitis.[40] Our results show that pro-inflammatory macrophages (Fig. 2(j)) have a higher NF-κB response under inflammatory conditions than inflamed epithelial cells (Fig. 2(k) and Fig. S3a) and ITMs and free RU.521 (at equivalent dose) both significantly downregulate NF-κB in these cells. It is worth noting that some cells, such as macrophages, have a high basal NF-κB level, which means control cells and LPS-stimulated cell lysates show the same levels of NF-κB.[41] Finally, ITMs' ability to suppress cGAS activation was evaluated in RAW 264.7 cGAS-knockout macrophages (RAW KO-cGAS), which have a luciferase reporter gene (ISG54) that responds to type-I interferon activation. RAW KO-cGAS cells were stimulated with cGAMP to activate the cGAS–STING pathway. ITMs significantly decreased the cGAS reporter gene activity (Fig. 2(l)) when cells were stimulated with cGAMP, and in the absence of cGAMP stimulation ITMs had minimal impact on the reporter activity. DCFDA was used to measure intracellular ROS in control *versus* inflamed cells with or without ITMs or free drug (Fig. 2(m) and (n)). J774A1 and MODE-k cells were incubated with LPS to induce inflammation and were subsequently incubated

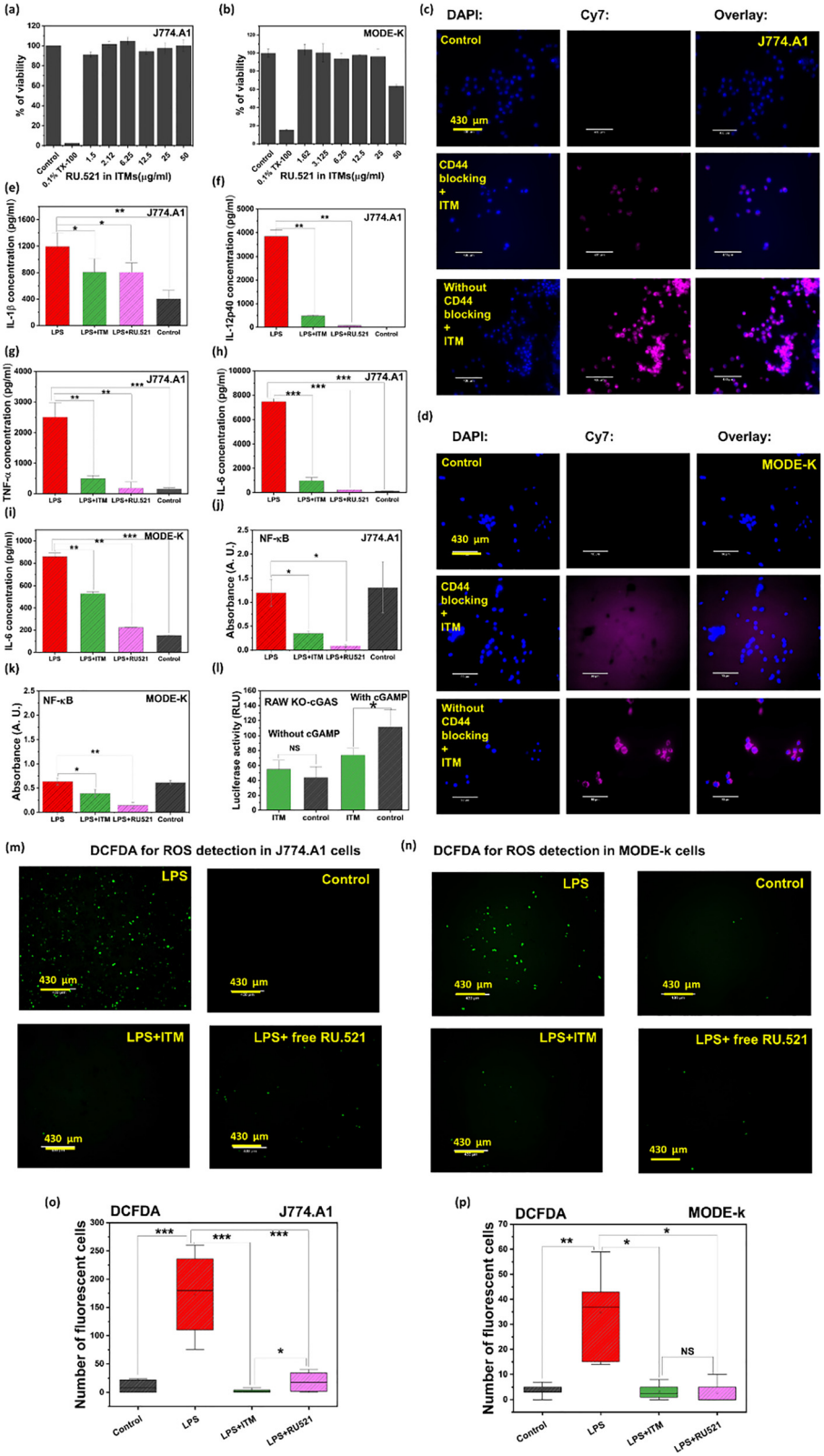

Fig. 2 *In vitro* activity of ITMs. (a) Cellular viability of J774.A1 macrophages treated with 100 μM RU.521 loaded ITMs and (b) Cellular viability of MODE-K epithelial cells treated with 100 μM RU.521 loaded ITMs. In both (a) and (b) untreated cells served as a negative control (*i.e.*, no cytotoxicity), and 0.1% Triton X-100 was chosen as the positive control for cytotoxicity. (c) Fluorescence images of internalization of IR780-loaded micelles in LPS-stimulated J774.A1 macrophages showing cells incubated without micelles (top), cells where CD44 receptors were blocked and incubated with micelles (middle), and cells without CD44 blocking and incubated with micelles (bottom). The scale bar is 430 μm. (d) Fluorescence images of internalization of IR780-loaded micelles in LPS-treated MODE-K epithelial cells incubated without micelles (top), cells where CD44 receptors were blocked and incubated with

micelles (middle), and cells without CD44 blocking and incubated with micelles (bottom). The scale bar is 430 μm. Cytokine analysis of culture supernatants from LPS-treated J774A.1 cells treated with ITMs and an equivalent dose of RU.521 (100 μM) alone. The cytokines analyzed include (e) IL-1β, (f) IL-12p40, (g) TNF-α and (h) IL-6. (i) Cytokine (IL-6) concentrations in LPS-treated MODE-K cell media treated with ITMs and an equivalent dose of RU.521 (100 μM) alone or untreated (LPS) control. (j) ELISA analysis of NF-κB concentration in LPS-treated J774.A1 cell lysates; here cells are treated with ITMs and an equivalent dose of RU.521 (100 μM) as free drug or untreated (LPS) control. (k) ELISA analysis of NF-κB concentration in LPS-treated MODE-K cell lysates; LPS-treated MODE-K cells were treated with ITMs or an equivalent dose of RU.521 (100 μM) as free drug or untreated (LPS) control. (l) Relative luciferase unit of RAW KO-cGAS cells with and without cGAMP stimulation and simultaneous treatment with RU.521 and ITMs. Intracellular ROS measured by DCFDA staining in (m) J774.A1 and (n) MODE-k cells in four groups that include treated with LPS, untreated control, LPS + ITMs, and LPS + free RU.521. Quantification of ROS in (o) J774.A1 and (p) MODE-k cells. Here, analyses were conducted with $n = 3$ samples per group. Statistical significance is reported by a 2-tailed Student's t-test $*p < 0.05$, $**p < 0.01$, $***p < 0.001$, and NS (not significant) $p > 0.05$.

with either ITMs or RU.521. The four groups of control, LPS, LPS + ITMs and LPS + RU.521 were then incubated with DCFDA and imaged live, which showed a significant decrease of ROS in cells that were incubated with either ITMs or RU.521 (Fig. 2(p) and (q)).

2.3. Therapeutic efficacy of ITMs in the *E. coli*-induced moderate colitis model *in vivo*

The effectiveness of ITMs was first evaluated in a moderate colitis model where both male and female ASF-IL-10 KO mice aged 11–16 weeks were colonized with *E. coli* 1D. Each mouse received 5×10^8 *E. coli* 1D *via* oral gavage on day 0 of the experiment. The disease progression is slow in this *E. coli* 1D model and an "inflammatory trigger" (*i.e.*, second hit) is needed to induce colitis that is representative of the more long-term progression noted for IBD patients. Here, mice were monitored for 3 weeks after the initial inoculation of *E. coli* 1D and then treated with ITMs daily for 2 weeks in a prophylactic setting (Fig. 3(a)). At 5 weeks post-inoculation, mice were given 2% dextran sulfate sodium (DSS) in drinking water for 5 days where DSS served as an inflammatory trigger inducing colitis in mice. ITM treatment was continued during the 5 days of DSS exposure. The effects of low percentage DSS dosage (1.5–2.5%) were examined in the ASF-IL10 KO mice (Fig. S4) and were found to induce very mild colitis (some colon shortening, no significant weight loss) with significantly less severity than when inoculated with *E. coli* 1D. The combination of *E. coli* 1D and 2% DSS (which is below the typical 4% of the DSS model) produced a gradual and sustained increase in inflammation followed by a mild flare that represented the development of mild colitis in humans. After 5 days on DSS, mice were euthanized on day 40 of the experiment, and tissues and fecal samples were collected.

Representative macroscopic images of the colon (Fig. 3(b)) from untreated, *E. coli* 1D-infected mice show no fecal pellet formation and a thickened (*i.e.*, edematous) colon that is characteristic of moderate colitis. ITM treatment protected mice from colon shortening and thickening (Fig. 3(c)), enabled defined fecal pellet formation (*i.e.*, sign of normal colon function), and also facilitated bodyweight recovery equivalent to the healthy mice (Fig. 3(d)). The standard deviation in the bodyweight measurement has resulted from the use of both male and female mice that respond differently to colitis-induced weight loss highlighting sex as a biological variable in colitis. We have previously shown that unencapsulated RU.521 as a free drug is not effective in attenuating intestinal inflammation relative to when loaded in micelles[22] and therefore free RU.521 was not included as a treatment group in this study. Well-established criteria for disease activity index (DAI)[42] were used including stool consistency, weight loss, rectal bleeding, mice posture and mobility, fecal pellet formation, and extent of colon shortening and thickening. ITM treatment improved the DAI of *E. coli* 1D infected mice (Fig. 3(e)) and reduced the symptoms of splenomegaly, *i.e.*, it decreased the spleen to bodyweight ratio (Fig. 3(f)). IBDs are associated with a decrease in the splenic function and enlargement of the spleen (splenomegaly). Splenomegaly occurs during systemic inflammation and immune activation, and is a common consequence of ulcerative colitis. A reduction in the spleen-to-body weight ratio indicates reduced systemic inflammation. The ITM treatment suppressed the systemic inflammatory response *via* inhibition of the cGAS–STING pathway, thereby reducing spleen enlargement. Lipocalin-2 levels in feces were also measured as a quantifiable indicator of murine typhlocolitis and as a biomarker for modest intestinal inflammation,[43] which indicated that ITMs reduced intestinal inflammation in mice (Fig. 3(g)). However, no differences in MPO were observed between untreated and ITM treated groups (Fig. 3(h)), which may be attributed to similar neutrophil infiltration in these groups, suggesting that neutrophil recruitment is not pathognomonic in the *E. coli* model. Further, the measurement of serum IFN-α in the treatment groups confirmed the downregulation of cGAS in the RU.521 loaded ITM group (Fig. 3(i)). We also measured fecal colony forming units (CFU) of *E. coli* to show that the treatment had no impact on the CFU of *E. coli* and the effect of ITMs was to attenuate the host inflammatory response (Fig. 3(j)). Fecal CFU tested in healthy ASF IL-10 KO mice showed no contamination with *E. coli*. The two groups that were infected with *E. coli* showed similar counts of CFU (not statistically significant). Thus, the benefits of the ITM treatment were mediated by cGAS inhibition and amelioration of intestinal inflammation rather than eradication of pathogenic bacteria.

2.4. Biodistribution of ITMs and therapeutic efficacy in *Helicobacter bilis*-induced severe colitis

Next the therapeutic ability of ITMs was evaluated in an *H. bilis* induced severe, acute colitis model where male and female ASF-IL-10 KO mice between the ages of 8 and 20 weeks were infected with *H. bilis*. In an ASF-IL-10 KO host with a compromised immune system, *H. bilis* induces severe colitis within a few days resulting in rapid deterioration of overall health. We first examined the biodistribution of ITMs in this model with the use of IR780-loaded micelles. Mice were monitored until early

clinical signs of colitis were noticeable (*e.g.*, weight loss, diarrhea) that occurred on day 5–7 post-infection. Mice were given a single oral dose of 10 μg IR780 loaded in micelles which enabled visualization of micelles *in vivo* and in tissues. Mice were euthanized at 24 h and 48 h post-administration of IR780-loaded micelles, and tissues were collected. Here, through

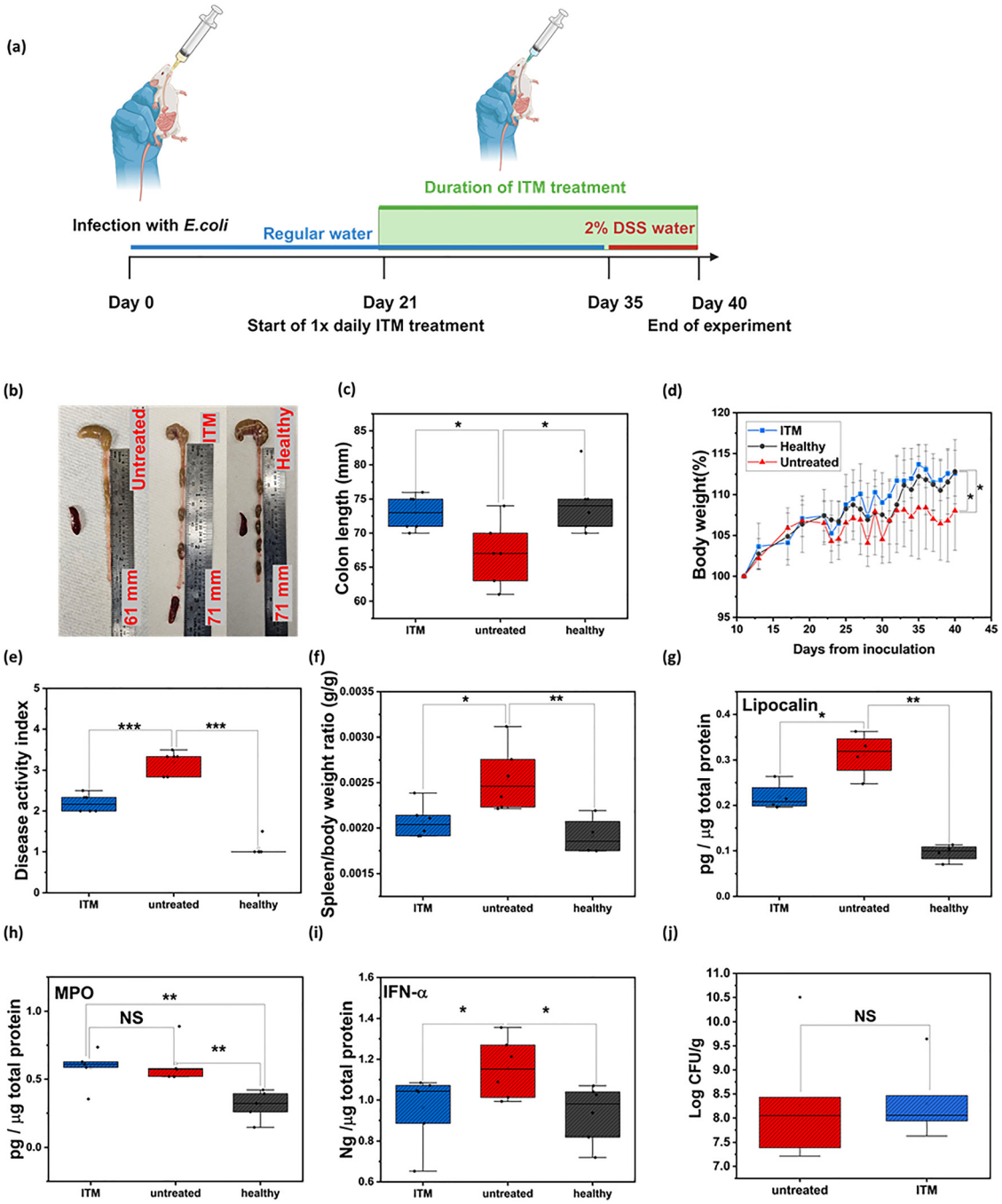

Fig. 3 *In vivo* therapeutic efficacy of ITMs in the *E. coli* 1D induced moderate colitis model. (a) Schematic showing the study design of the moderate colitis model. Created in **https://BioRender.com** (b) Representative images of the colon and spleen of mice infected with *E. coli* 1D: untreated (infected), or infected and treated with ITMs, as well as from healthy mice. (c) Colon length of the different groups and (d) normalized bodyweight percentage. The standard deviation in the bodyweight measurement has resulted from the use of both male and female mice that respond differently to colitis-induced weight loss highlighting sex as a biological variable in colitis. (e) Disease activity index, (f) spleen to bodyweight ratio, (g) amount of lipocalin (pg) normalized to total protein (μg) in colon lysates, (h) MPO activity in colon lysates normalized to total protein, and (i) ELISA analysis of IFN-α concentration in mouse sera. (j) Fecal colony-forming units (CFU) of mice infected with *E. coli* 1D and untreated, and those treated with ITMs. The error bar in all panels represents $n = 5$ mice per treatment group . Statistical significance is reported by a 2-tailed Student's *t*-test $^{*}p < 0.05$, $^{**}p < 0.01$, $^{***}p < 0.001$, and NS (not significant) $p > 0.05$.

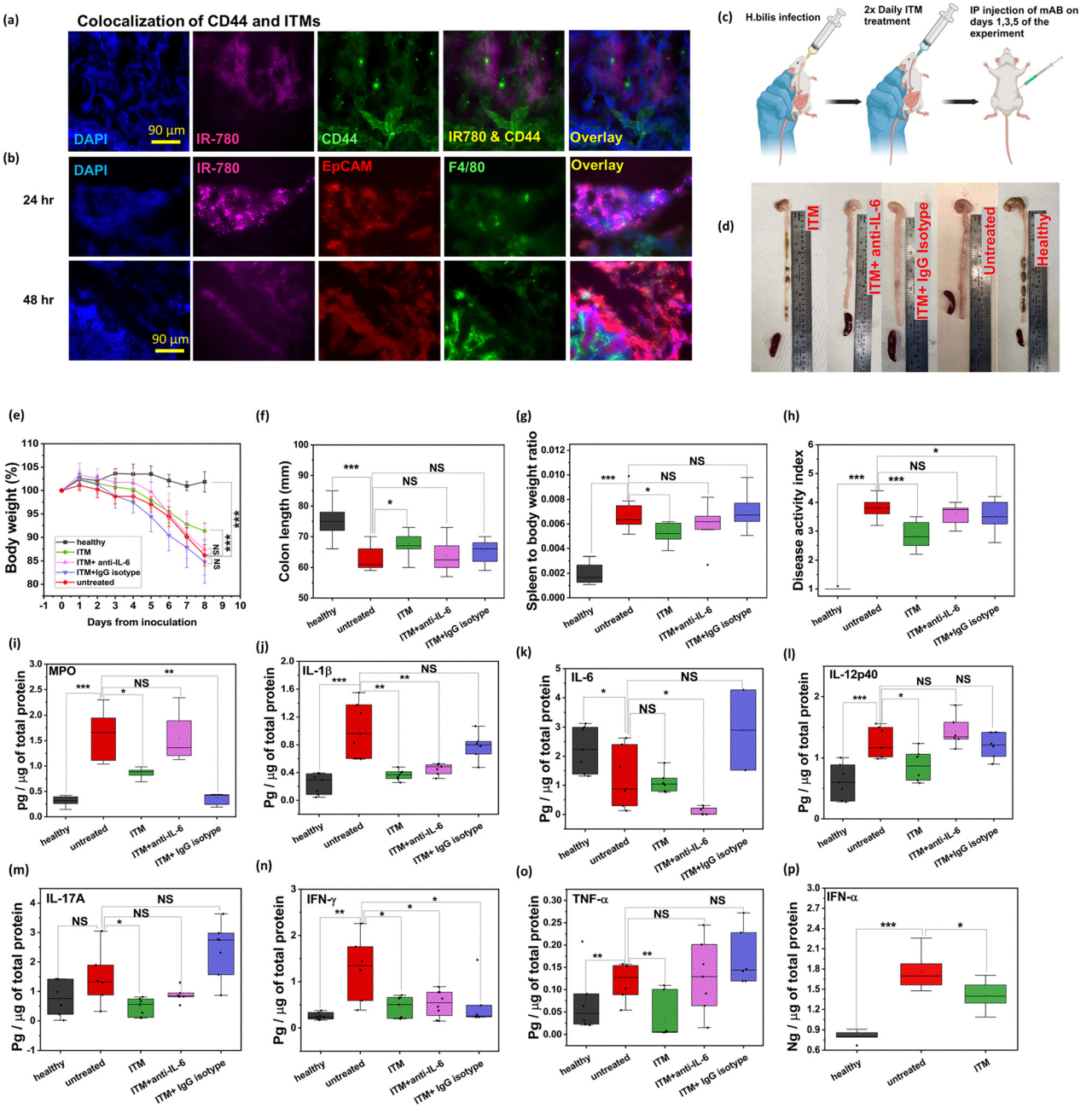

Fig. 4 *In vivo* therapeutic efficacy of ITMs in the *H. bilis* induced severe, acute colitis model. (a) Colocalization of CD44 and ITMs. From left to right, DAPI in blue, IR780 loaded micelles in magenta, CD44 in green, overlay of CD44 and IR780 and overlay of all three channels. (b) Fluorescence photomicrographs of *H. bilis* infected mouse colon: 24 h (top) and 48 h (bottom) after receiving a dose of IR780-loaded micelles. From left to right, DAPI in blue, IR780 loaded micelles in magenta, EpCAM-labeled IECs in red, F4/80-labeled macrophages in green and overlay of all four channels. (c) Schematic showing oral gavage of ITMs and IP injection of mAb. Created in **https://BioRender.com**. (d) Photos of the colon and spleen of mice from different treatment groups demonstrating the efficacy of ITMs and combination therapies. (e) Daily weight percent normalized to the starting weight for ASF IL-10KO mice in different treatment groups. All mice except the healthy group were colonized with *H. bilis* at the start of the experiment: healthy, untreated (colitis), ITMs, ITMs + IgG isotype control, ITMs+ anti-IL-6. (f) Colon length, (g) spleen weight to body weight ratio, (h) disease activity index (DAI), and (i) myeloperoxidase (MPO) activity in colon tissue normalized to total protein for the different treatment groups. Cytokine analysis in colonic explant media which includes (j) IL-1β, (k) IL-6, (l) IL-12p40, (m) IL-17A, (n) IFN-γ, and (o) TNF-α, and (p) ELISA analysis of IFN-α concentration in mouse sera indicating systemic STING inhibition. The error bar in all panels represents n = 5–6 mice per treatment group. Statistical significance is reported by a 2-tailed Student's t-test $^{*}p < 0.05$, $^{**}p < 0.01$, $^{***}p < 0.001$, and NS (not significant) $p > 0.05$.

immunofluorescence staining with CD44, we have shown high CD44 expression in the inflamed colon and that ITM uptake in the inflamed colon is facilitated through CD44-HA binding (Fig. 4(a)). We have also shown time dependent uptake of ITMs *in vivo* in our previous work with IVIS imaging.[22] Next, with longitudinal immunofluorescence (IF) images of colon tissues

stained for EpCAM (inflamed epithelial cells), F4/80 (macrophages), and DAPI, we aimed to determine which cell types in the inflamed colon did the micelles associate with, and if such association was time-dependent. Our findings show that at 24 h post-administration of the IR780-loaded micelles, micelles are accumulated in the colon (Fig. 4(b), IR780 panel), and it is evident that micelles are localized with both macrophages (Fig. 4(a), F4/80 panel) and inflamed epithelial cells (Fig. 4(a), EpCAM panel) in the colon and the drug is released at the site of inflammation at this time point. At 48 h post-administration the IF images show that the fluorescence intensity of micelles is significantly reduced and is also more dispersed suggesting that micelles start clearing from the colon by this time point.

Next the therapeutic efficacy of ITMs and their ability to downregulate cGAS–STING signaling were evaluated in the *H. bilis* induced severe colitis model with both male and female ASF-IL-10 KO mice. Mice were infected on day 0 and from day 1 mice were administered two oral doses of ITMs daily (Fig. 4(c)), with each 250 μL oral dose of ITMs containing 100 μM encapsulated RU.521. Multidose therapy both in mouse models of acute colitis[44,45] and in patients[46,47] with moderate to high disease severity has shown to reduce macroscopic and microscopic signs of disease, and therefore, we orally administered dual therapeutic doses of ITMs. We compared the *in vivo* efficacy of ITMs alone and in combination with anti-IL-6 mAbs. It has been previously shown that downregulation (*i.e.*, neutralization) of mucosal IL-6 minimizes disease severity mediated by pathogenic bacteria; furthermore, anti-IL-6 mAb treatment is approved in colitis patients.[48,49] We hypothesized that the use of combination therapy with ITMs + anti-IL-6 would attenuate colitic lesions and reduce the inflammatory response enabling bodyweight recovery and protecting mice from severe colitis (*e.g.*, colon shortening). As a control, ITMs were combined with a non-specific IgG to match the isotype of anti-IL-6. In each case, 300 μg of mAbs was administered *via* intraperitoneal (IP) injection on days 1, 3, and 5 after infection. Representative images of the colon, caecum, and spleen from a representative mouse in each treatment group (Fig. 4(d)) indicate the degree of disease as assessed by shortened colon, thickened (*i.e.*, edematous) colon, atrophied and swollen caecum, splenomegaly, and absence of the characteristic ''string of pearls'' fecal pellet formation (*i.e.*, loss of distal colon function).[50] Our findings suggest that ITMs may have more benefits on the colon as opposed to the caecum. Treatment with ITMs alone shows better fecal pellet formation, albeit small, and reduced colonic edema relative to the untreated group as well as those treated with anti-IL-6. The percentage bodyweight of mice normalized to their bodyweight at day 0 (Fig. 4(e)) shows that relative to the other treatment groups, ITMs alone had a slower bodyweight loss as evidenced by the slope of the weight loss. This is also consistent with the colon images which show that ITM treated mice had less edema and have some content suggesting more normal fluid recovery. As colon shortening is a characteristic feature of murine colitis, the colon length was measured from the proximal end of the caecum to the distal end of the rectum (Fig. 4(f)). The ITM treatment group had longer colons than the untreated and other treatment groups, indicating that ITM treatment attenuated colon shortening resulting from *H. bilis* infection. Our results show (Fig. 4(g)) reduction in the spleen to bodyweight ratio for the mice treated with ITMs relative to the other treatment groups. The disease activity index (DAI) was also assessed from all of the mice in this study ($n \sim 15$/group) and scored on a range of 1 to 5, with 1 being healthy and 5 being high disease activity with the same criteria as mentioned in Fig. 3 discussion (Fig. 4(h)). ITM treatment resulted in a significantly lower DAI relative to the other treatment groups. Combination treatment of ITMs with anti-IL-6 mAbs had a detrimental effect in mice as observed in the lack of bodyweight recovery, colon shortening, high spleen to bodyweight ratio, and no improvement in DAI. This unexpected finding is further discussed below with cytokine analysis. The myeloperoxidase (MPO) activity was also evaluated in homogenized colon samples (Fig. 4(i)); MPO catalyzes the production of ROS contributing to inflammation and is correlated with neutrophil infiltration in colitis.[51] Treatment with ITMs alone and combination of ITMs + IgG isotype control both showed a decrease in MPO. ITMs' ability to reduce proinflammatory cytokines was also evaluated as a quantitative measure of attenuation of colonic inflammation (Fig. 4(j)–(o)).[52] ITMs significantly decreased several cytokines including IL-1β, IL-12p40, IL-17A, IFN-γ and TNF-α relative to other treatment groups. IL-6 has a complex role in the ASF IL-10 KO model, which has a different immune system than conventional mice because of the lack of IL-10. Despite the proinflammatory characteristic of IL-6, a high level of this cytokine is observed in the non-infected group in comparison to the untreated colitis group, which could be attributable to the basal low-grade inflammation characteristic of ASF IL-10 KO mice (Fig. 4(k)). Moreover, IL-6 is a pleiotropic cytokine where a certain level is necessary to maintain gut homeostasis.[53] IL-6 also helps in intestinal epithelial cell restitution and regulates intestinal epithelial tight junctions, which further explains why anti-IL-6 treatment can be detrimental in an *H. bilis* infection model.[53,54] Finally, systemic inhibition of cGAS expression was also confirmed by quantifying IFN-α, a type 1 interferon downstream of the activation of the cGAS–STING pathway.[55] Lower levels of serum IFN-α indicate downregulation of cGAS in the ITM group relative to untreated, infected mice (Fig. 4(p)).

2.5 Therapeutic efficacy of ITMs in combination with anti-IL-12p40

Due to the severity of colitis in the *H. bilis* model, few treatments allow complete response in this model. Recent studies have shown that IL-12 and IL-23 cytokines aid and perpetuate intestinal inflammation, where IL-12 promotes the differentiation of naïve T cells in Th1 effectors and IL-23 increases the proinflammatory functions of Th17 cells.[56] Immunotherapies (*i.e.*, monoclonal antibodies) directed against the shared p40 subunit of IL-12 and IL-23 have shown efficacy in pilot studies and clinical trials (NCT03167437, NCT01369355, *etc.*).[36,57,58] Further, IL-10 deficient mice also have an aberrant response of $CD4^+$ T cells and secrete more proinflammatory cytokines

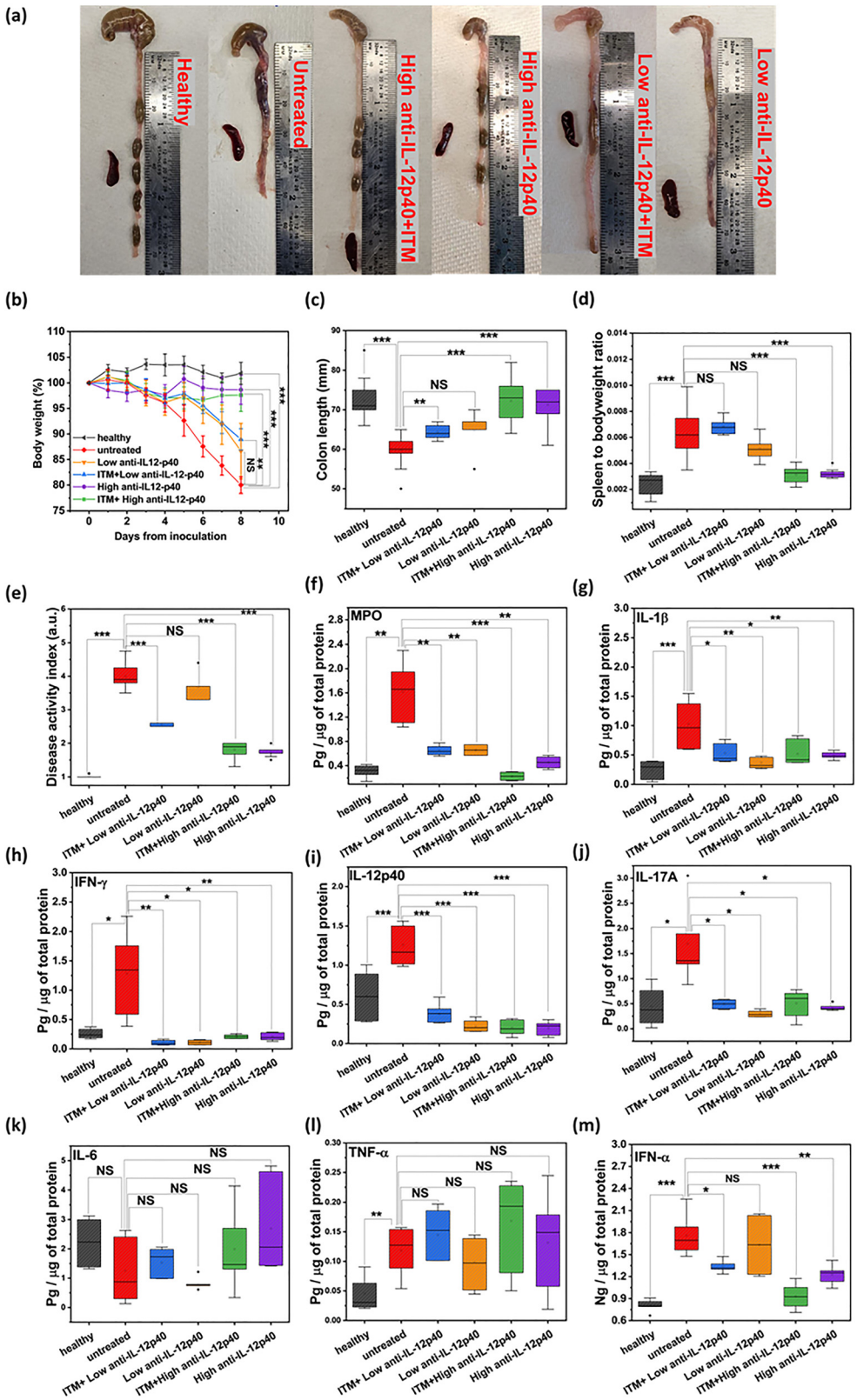

Fig. 5 *In vivo* efficacy of ITMs in combination with anti-IL-12p40 in ASF IL-10 KO mice infected with *H. bilis*. (a) Representative colon and spleen images of treatment groups that include healthy, untreated (*H. bilis* infected), ITM + high anti-IL-12p40 (3 × 300 μg mAbs), high anti-IL-12p40 (3 × 300 μg mAbs), ITM + low anti-IL-12p40 (3 × 10 μg mAbs) and low IL-12p40 (3 × 10 μg mAbs). (b) Normalized daily bodyweight percentage for healthy, untreated, and mice treated with the different treatment groups. The error bar in these panels represents n = 8 mice per treatment group. (c) Colon length, (d) spleen to body weight ratio, (e) disease activity index, and (f) MPO normalized to total protein of mice in different treatment groups. Cytokine analysis in colonic explant media which includes (g) IL-1β, (h) IFN-γ, (i) IL-12p40, (j) IL-17A, (k) IL-6, and (l) TNF-α, and (m) ELISA analysis of IFN-α concentration in mouse sera for the treatment groups. Statistical significance is reported by a 2-tailed Student's t-test $^{*}p < 0.05$, $^{**}p < 0.01$, $^{***}p < 0.001$, and NS (not significant) $p > 0.05$.

such as IL-12, IL-17 and IFN-γ.[2] Thus, we hypothesized that the inhibition provided by anti-IL-12p40 combined with ITM treatment would attenuate colitic lesions and reduce the inflammatory response improving the overall gut health of mice. Note that combination therapies are now adopted in clinical practice for patients with high disease severity and those that acquire resistance to initial monotherapies.[35,36]

Here both a high dose of anti-IL-12p40 at 300 μg (dose equivalent to anti-IL-6 and IgG isotype control shown in Fig. 3) and a low dose at 10 μg were evaluated and combination treatment was compared to monotherapies with mAbs alone. Mice were infected with *H. bilis* on day 0 of the experiment; for groups that received combination treatment of anti-IL-12p40 + ITMs, the mice were administered two oral doses of ITMs daily beginning on day 1 after infection, followed by a high or low dose of anti-IL-12p40 *via* I.P. injection on days 1, 3 and 5 following the colonization with *H. bilis*. Mice were euthanized at the end of the study period when one of the groups had reached 80% of starting bodyweight. Based on our findings using the high dose of anti- IL-12p40 (300 μg), the therapeutic benefit of mAb alone and ITMs + anti-IL-12p40 was similar in terms of improved colon morphology and presence of formed fecal pellets but with some cecal atrophy (Fig. 5(a)). The high dose of anti-IL-12p40 with and without ITMs also showed effective bodyweight recovery, maintained colon length, and showed lower DAI, lower level of MPO activity, and lower levels of cytokines (Fig. 5(b)–(l)). We note that ITM treatment alone also significantly reduced IL-12p40 and IL-17A levels (Fig. 4) suggesting that inhibition of the cGAS–STING pathway converges on IL-12/IL-23p40 activity and therefore the combination treatment of ITMs + anti-IL-12p40 should have a more effective therapeutic impact. The complementary effect of the cGAS–STING pathway and IL-12/IL-23p40 activity can be explained through NF-κB activation. STING signaling activates NF-κB,[5] which in turn binds to the IL-12p40 promoter and activates gene expression, thus upregulating IL-12/23 activity.[59,60] This hypothesis is further confirmed through the analysis of serum IFN-α (Fig. 5(m)) which shows that both high dose anti-IL-12p40 mAbs alone and in combination with ITMs lead to the downregulation of IFN-α.

In comparison to mice that were treated with the low dose of anti-IL-12p40 (10 μg) alone, the combination treatment of ITMs + low dose mAbs shows a clear advantage in bodyweight recovery, maintenance of colon length, and in the overall macroscopic appearance of the colon. Mice treated with low mAbs alone presented severe rectal bleeding, lethargy, and hunched posture while the GI tract of mice that received combination therapy appeared healthier and the mice were overall more active as reflected in their DAI (Fig. 5(e)). This suggests that combination treatment may enable the use of significantly lower doses of mAbs minimizing the high costs and unnecessary side effects associated with the use of mAbs. Both mAbs alone and combination treatment groups had significantly lower MPO activity and lower amounts of most proinflammatory cytokines, indicating the effectiveness of this treatment combination to prevent severe colitis. The IL-6 responses observed (Fig. 5(k)) are not surprising as explained earlier in Fig. 4. Similarly, the TNF-α responses observed (Fig. 5(l)) are likely because TNF-α increases immediately following an inflammatory response, but in cases of chronic inflammation such as in the *H. bilis* model, the levels of TNF-α had already subsided such that differences among the treatment groups were not distinguishable. We also assessed the use of an intermediate dose of anti-IL-12p40 (3 × 50 μg) alone and in combination with ITMs (Fig. S5) and examined the longevity of mice for up to 14 days post-infection with *H. bilis*. Our results indicate that whereas the mice in the infected only group had lost >20% of bodyweight by day 8 and were humanely euthanized, the mice in both the mAbs alone and combination treatment groups had maintained bodyweight through day 13 post-infection and had colon length and DAI similar to that of the healthy mice.

The *in vivo* endpoints were further confirmed with *ex vivo* analysis of colon tissues *via* histopathological evaluation (Fig. 6) and immunofluorescence (IF) staining (Fig. 7). The histopathological scores were generated by blinded evaluation performed by a board-certified anatomic veterinary pathologist on $n = 3$ colon tissues per group. A specific semi-quantitative histopathologic scoring system, detailed in the materials and methods section (Section 4), was developed and applied throughout. This scoring system evaluated tissue damage (superficial to transmural), the extent of inflammation (superficial to transmural), severity of inflammation in the lamina propria, submucosa, and muscularis/serosa, epithelial change (erosion, ulceration, crypt loss, hyperplasia), and edema. Scores (1–5) for each parameter were summed up for each individual mouse to obtain a total histopathologic score (THS, 24 possible points/mouse). The THSs were averaged by treatment group and detailed by the criterion in Fig. S6a–f. Histological assessment showed that mice in the healthy (PBS only) group had none to moderate histological lesions with intact colonic epithelium (black arrows). No to minimal inflammation was observed in the lamina propria, submucosa, or tunica muscularis/serosa (Fig. 6(a)). In contrast, the untreated mice infected with *H. bilis* (Fig. 6(b)) had severe histological lesions that were characterized by eroded or ulcerated surface epithelium extending over numerous crypts, marked crypt loss (greater than 50%) and markedly hyperplastic remnant crypts (black arrows). Inflammation was transmural and characterized by moderate intraluminal fibrinoneutrophilic exudate (yellow asterisk), severe fibrinoneutrophilic to lymphoplasmacytic inflammation in the lamina propria (black asterisk), moderate to severe lymphohistiocytic inflammation in the submucosa (black vertical bar), and perivascular to interstitial lymphoplasmacytic inflammation in the muscularis and serosa. All treated groups demonstrated a significant reduction in the average THS when compared to the untreated group. Mice treated with ITMs (Fig. 6(c)), ITMs + high anti-IL-12p40 (Fig. 6(d)), ITMs + low anti-IL-12p40 (Fig. 6(f)), and low anti-IL-12p40 (Fig. 6(g)) had similar histopathological changes and presented moderate lesions. Histopathologic changes were characterized by erosion of the surface epithelium, no to minimal ulceration, minimal colonic crypt loss (5–10%), and scattered

crypt abscesses (yellow arrowheads). Inflammation was mostly limited to the mucosa and submucosa as opposed to the untreated group which exhibited inflammation in the muscularis and serosa. Neutrophilic inflammation with lymphohistiocytic aggregates was observed in the lamina propria (black asterisk). Interstitial to perivascular lymphoplasmacytic aggregates with edema were observed in the submucosa (black vertical bars). Scattered perivascular lymphoplasmacytic infiltrates were observed in the outer intestinal layers. The high anti-IL-12p40 treated group (Fig. 6(e)) had a moderate mean THS. Histopathological changes in this group were characterized by erosion of the surface epithelium without ulceration and limited crypt changes consisting of mild hyperplasia (arrowhead). Inflammation was limited to the mucosa and submucosa. Moderate neutrophilic inflammation was observed in the lamina propria with mild to moderate interstitial to perivascular lymphoplasmacytic aggregates in the submucosa (black vertical lines). These findings indicate the significant benefit of ITMs + anti-IL-12p40 combination treatment at appropriate doses related to disease severity. Histopathological evaluation and semi-quantitative analysis of the colon tissues that were treated with 50 μg dose of anti-IL-12p40, ITMs + anti-IL-6, and ITMs + IgG groups are provided in Fig. S6.

Further, IF images of tissues were obtained where tissues were stained with mAbs specific for macrophages (F4/80), epithelial cells (epithelial cell adhesion molecule, EpCAM), a tight junction protein (zonula occludens-1, ZO-1), and STING protein to evaluate if the intestinal tissue is intact and STING is being downregulated with the ITM treatment. Our findings show that the colon of mice in the untreated, infected group had high macrophage infiltration (Fig. 7(a)) characteristic of chronic inflammation. The healthy and all treatment groups had minimal macrophage recruitment. It is noteworthy that while macrophage migration is vital for restitution of inflamed tissue, prolonged state of inflammation in the absence of regulatory T cells (T_{regs}) in the ASF IL-10 KO mice results in aberrant immune response. EpCAM, a type I transmembrane glycoprotein, is responsible for cell signaling, cell adhesion,

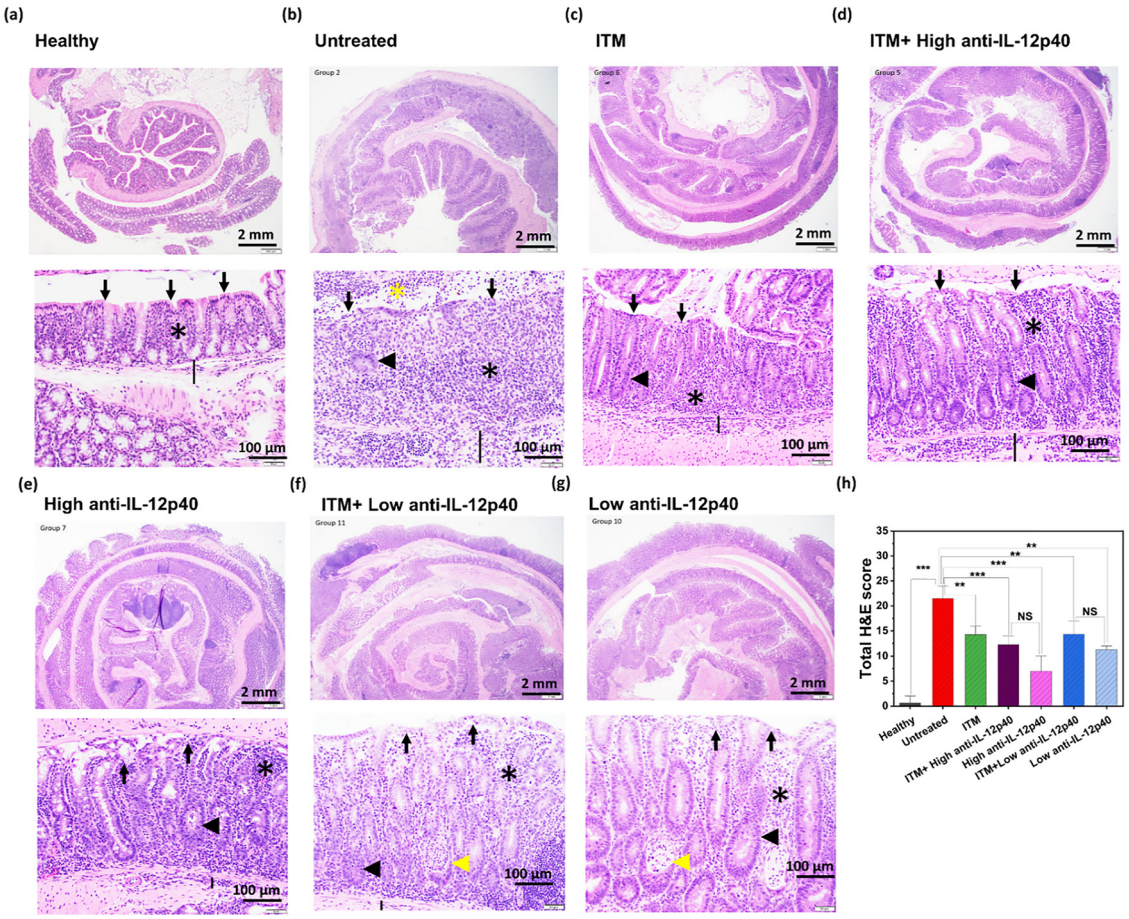

Fig. 6 *Ex vivo* analysis of colon tissues from *H. bilis* colonized and healthy mice. (a)–(g) Low magnification (top row) and high magnification (bottom row) photomicrographs of hematoxylin and eosin (H&E) stained histopathological sections of the colon for different treatment groups (top row: healthy, untreated (*H. bilis* infected), ITM, ITMs + high anti-IL-12p40 (300 μg), high anti-IL-12p40 alone, ITMs + low anti-IL-12p40 (10 μg), and low anti-IL-12p40 alone. The colonic surface epithelium (black arrows), lamina propria (black asterisk), submucosa (black vertical bar), hyperplastic colonic glands (black arrowheads), crypt abscesses (yellow arrowheads), and intraluminal exudate (yellow asterisks) are highlighted in each image. The scale bar is 2 mm (low magnification) and 100 μm (high magnification) for panels (a)–(g). (h) Quantitative total H&E scores for treatment groups for $n = 3$ tissues per group. Statistical significance is reported by a 2-tailed Student's *t*-test $^{*}p < 0.05$, $^{**}p < 0.01$, $^{***}p < 0.001$, and NS (not significant) $p > 0.05$.

and maintenance of the epithelial barrier function.[61] ZO-1, a peripheral membrane protein, is only present in intact epithelium and is also involved in maintaining the intestinal mucosal barrier function as part of the tight junction complex which protects the body from the luminal contents of the gut.[62–64] Our IF analysis shows that both EpCAM and ZO-1 (Fig. 7(b) and (c)) had low IF signal in the colonic tissue of untreated, *H. bilis* infected mice relative to the healthy tissues and those in the treated groups. This suggests an increase in erosion and ulceration of the epithelial barrier in the untreated mice which is less prominent post-treatment with ITMs, anti-IL-12p40, and ITMs + anti-IL-12p40 combination. IF images of STING

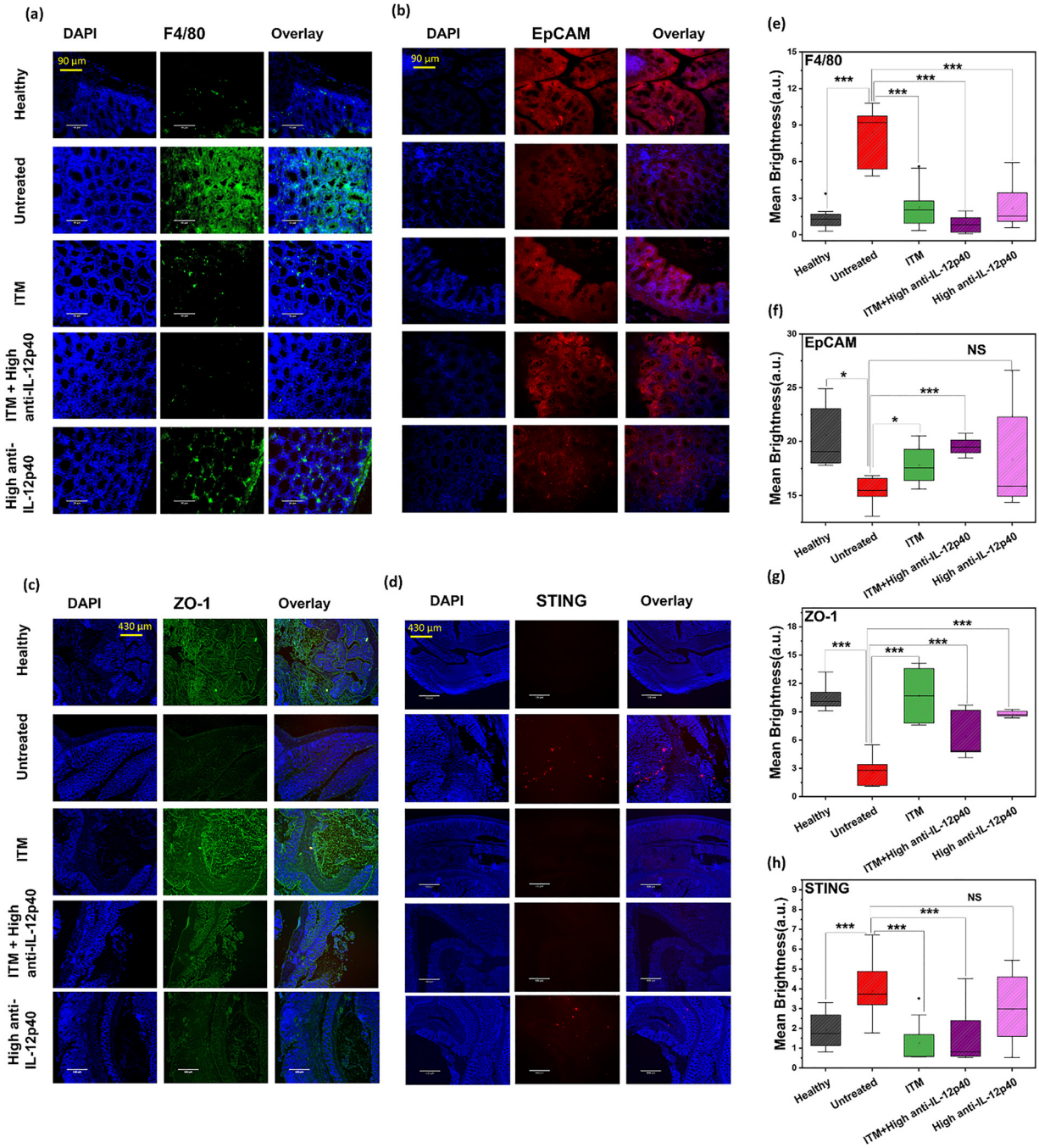

Fig. 7 *Ex vivo immunofluorescence* analysis of colon tissues of ITM treated and combination treatment mice infected with *H. bilis*. Immunofluorescence images of colon tissues showing (a) F4/80 (green) macrophage marker, (b) EpCAM (red) epithelial cell marker, (c) ZO-1 (green) tight junction protein marker, and (d) STING (red). Groups from top to bottom in each panel: healthy, untreated, ITMs alone, ITMs + high dose anti-IL-12p40, and high dose anti-IL-12p40 alone. Quantification of the average fluorescence signal for each marker represented in the images including (e) F4/80, (f) EpCAM, (g) ZO-1, and (h) STING for $n = 3$ tissues per group. Statistical significance is reported by a 2-tailed Student's *t*-test $^{*}p < 0.05$, $^{**}p < 0.01$, $^{***}p < 0.001$, and NS (not significant) $p > 0.05$.

expression in colon tissues show upregulation in the untreated colitis group and successful downregulation of STING in the ITMs alone and combination treatment groups (Fig. 7(d)). The quantification of F4/80, EpCAM, ZO-1, and STING in IF images for $n = 3$ mice per group is shown in Fig. 7(e)–(h).

3. Conclusions

In summary, this work demonstrates the therapeutic potential of cGAS inhibitor-loaded ITMs to attenuate inflammatory responses both *in vitro* (*e.g.*, macrophages and epithelial cells) and *in vivo* in two distinct microbial models of severe and moderate colitis. ITMs showed targeted uptake in the inflamed colon *via* HA-CD44 binding and also enabled ROS-responsive drug release, mediated by the thioketal linker at the site of inflammation. The ITMs were shown to suppress induction of key inflammatory cytokines *in vitro*. Using immunocompromised ASF-IL-10 KO mice, the ITMs were shown to attenuate the severity of colitis in mice that were infected with *H. bilis* or *E. coli*. Our findings show that ITM treatment alone effectively attenuated moderate colitis, and in the severe colitis model, disease severity was ameliorated with a combination of ITMs + anti-IL-12p40 recapitulating the efficacy of advanced combination therapies in patients with severe, acute disease. Our findings also show high levels of STING expression in tissues and systemic IFN-α in sera in both severe and moderate colitis models, suggesting the uncontrolled activation of the cGAS–cGAMP–STING pathway in IBDs. Further, downregulation of cGAS with ITMs and targeted mAbs directed against the shared p40 subunit of IL-12 and IL-23 presents a promising approach to regulate local inflammation. These findings underscore the therapeutic promise of ITM based combinatorial treatments in modulating inflammatory pathways, reducing recruitment of inflammatory cells, and enhancing mucosal integrity in colitis. We envision that novel ITMs that can be delivered orally and target areas of inflammation will enable an unprecedented approach to targeted drug delivery at the site of inflammation, minimizing systemic side effects and improving gut health and quality of life for IBD patients.

4. Materials and methods

4.1. Materials

Hyaluronic acid (HA) (100 kDa) was purchased from Lifecore Biomedical (USA) and stearic acid (SA) was purchased from Alfa Aesar (USA). Cysteamine, acetone, formamide, 1-ethyl-3-(3-dimethylaminopropyl) carbodiimide (EDC), *N*-hydroxysuccinimide (NHS), sodium hydroxide (NaOH), RU.521, 2,2′-azobis(2-amidinopropane) dihydrochloride (AAPH), sodium hypochlorite (NaOCl), hydrogen peroxide (H_2O_2), dichloromethane (DCM) and IR780 iodide were bought from Sigma-Aldrich (USA). *N*-*N*-Dimethyl formamide was bought from Merck (Germany).

4.2. Methods

4.2.1. Synthesis of the thioketal linker and ITMs. The synthesis of the thioketal linker followed a previously established method.[22] In summary, cysteamine (100 mmol) was dissolved in anhydrous acetone (269 mmol), saturated with dry hydrogen chloride, and stirred continuously for 8 hours at 23 °C. The resulting compound was washed twice with chloroform and then dried. Following this, the product was recrystallized in 6 N NaOH solution, repeating the process three times. Finally, the purified product was extracted with dichloromethane (DCM), yielding an 80% recovery. The NH_2–TK–SA–HA polymer was synthesized through a two-step procedure, with each step carried out in a three-neck round-bottom flask submerged in an oil bath, attached to a reflux condenser, and flushed with nitrogen gas. In the first step, stearic acid (SA) was conjugated to the thioketal linker *via* an EDC/NHS reaction, utilizing the amine ($-NH_2$) group on the linker and the carboxyl (–COOH) group on SA. To begin, SA (198 mg) was dissolved in 18 mL of DMF, followed by the addition of EDC (266 mg) and NHS (160 mg), with stirring for 30 minutes to initiate activation. Then, the TK linker (135 mg), dissolved in 2 mL of formamide with 97 μL of triethylamine, was added, and the reaction mixture was stirred overnight. The resulting compound was dialyzed (MWCO 3500 kDa) against distilled water for 24 hours and lyophilized. In the second step, hyaluronic acid (100 mg) was dissolved in 10 mL of formamide at 60 °C. Once dissolved, EDC (51 mg) and NHS (30 mg) were added, and the solution was stirred under nitrogen for 30 minutes. Subsequently, 36.5 mg of SA–TK dissolved in 2 mL of warm DMF was introduced, and the mixture was stirred for 16 hours under nitrogen flow. The solution was then dialyzed against distilled water and lyophilized to yield the NH_2–TK–SA–HA polymer in a dry form.

4.2.2. Synthesis of ITMs. RU.521 loaded ITMs were prepared by the dialysis method. Briefly, 10 mg of NH_2–TK–SA–HA was dissolved in 13 mL of distilled water (DW) and 2 mg of RU.521 in 1 mL of DMSO was added dropwise under sonication (amplitude 50%). After 5 min of sonication, the solution was subjected to dialysis (MWCO 100 kDa) against distilled water for 24 h. After dialysis, the resulting solution was filtered with Whatman filter paper and lyophilized. The same methodology was used to prepare IR780 loaded micelles. The RU.521 amount was determined by using UV-visible spectroscopy in dimethyl sulfoxide (DMSO). In order to find the drug loading content, a standard curve was generated for RU.521 in dimethyl sulfoxide (DMSO) in a range of concentrations. The drug loading content was calculated as per the following equation:

$$\text{Drug loading content } (\%) = \frac{\text{The amount of the loaded RU.521 in ITMs}}{\text{The amount of the ITMs}} \times 100.$$

4.2.3. Characterization. The chemical structure of NH_2–TK–SA–HA was confirmed by proton nuclear magnetic resonance (^{1}H NMR) spectroscopy (400 Hz, Bruker; Billerica, MA, USA). 10 mg of polymer was solubilized in DMSO-d6 : D_2O 7 : 1. Pyrene was used as a fluorescent probe to measure the critical micellar concentration (CMC). The ITM's average hydrodynamic diameter and zeta potential were measured by the

dynamic light scattering technique (DLS) using Zetasizer Nano Z (Malvern Instruments, Malvern, UK). All samples were analyzed in triplicate (n = 3). The morphology of the ITM was evaluated using a transmission electron microscope (TEM) (200 kV JEOL 2100, JEOL Ltd, Japan) with 2% uranyl acetate staining.

4.2.4. ROS responsiveness of ITMs. 1.5 mg mL^{-1} of ITMs was resuspended in PBS and incubated with or without 100 mM peroxy radical-generating reagent AAPH, 5 mM H_2O_2, and 1 mM NaOCl and incubated for one hour at 37 °C. After the incubation, the average hydrodynamic diameter and polydispersity index (PDI) were monitored by DLS.

4.2.5. *In vitro* release of RU.521. To evaluate the release of RU.521 from the ITMs, the samples were placed in dialysis bags, sealed, and kept in 30 mL of release medium (1× PBS) and incubated at 37 °C with shaking at 200 rpm. An appropriate amount of H_2O_2 was added to the release media to mimic the intracellular ROS environment to attain a final H_2O_2 concentration of 10 mM and 5 mM. One ml of the release medium was collected at different time intervals and substituted with an equivalent volume of fresh medium also at 37 °C. To transfer RU.521 out of the aqueous phase, 1 mL of dichloromethane (DCM) was added to each sample and vigorously vortexed to extract RU.521 into DCM. The DCM phase containing RU.521 was separated, and DCM was dried off overnight, and then the concentration of RU.521 was determined through UV-visible spectroscopy in DMSO.

4.2.6. Stability studies in simulated gastrointestinal fluids. To check the stability of ITMs in gastrointestinal fluids and enzymes, ITMs were incubated in simulated gastric fluid (SGF, pH 1.0–1.4, Ricca Chemical Company, Arlington, TX) containing 3.2 g L^{-1} pepsin, in simulated intestinal fluid (SIF, pH 7.4–7.6, Ricca Chemical Company, Arlington, TX) supplemented with pancreatin (10 g L^{-1}) and in PBS. Briefly, 1.5 mg mL^{-1} of lyophilized ITMs was resuspended in 1× PBS and placed in a dialysis bag (molecular weight cut-off (MWCO): 40 kDa). To evaluate the changes in ITMs upon moving from the stomach to intestine, the ITMs were first incubated in SGF + pepsin for 2 hours and then transferred to SIF + pancreatin and incubated for 6 hours. At specific time points, 1 mL of the medium was collected and replaced with an equivalent volume of fresh medium. Dichloromethane (DCM)-based extraction was employed to isolate RU.521. After the end of the experiment, dialysis bags were opened and dynamic light scattering (DLS) was performed to determine the average hydrodynamic diameter of the ITMs inside the dialysis bags.

4.2.7. Cellular viability and uptake of ITMs. *In vitro* cellular viability of ITMs was evaluated in mouse macrophage cell line J774.A1 and murine intestinal epithelial cell line MODE-K using the same protocol. Briefly, 5 × 10^4 cells per mL were seeded in a 96-well plate and incubated at 37 °C for 16 h. Subsequently, free RU.521, Triton-X100 and ITMs at various concentrations were added and incubated for 24 h. After 24 h of incubation, the cell viability was quantified using Dojindo Labratories' CCK-8 assay (code: CK04, LOT: TM673), as per the manufacturer's protocol.

To investigate the cellular uptake of IR780-loaded ITMs in LPS-TREATED macrophages, 5 × 10^4 cells per mL (either J774.A1 or MODE-K) were seeded in Lab-Tek® chamber slides in media containing 100 ng mL^{-1} of lipopolysaccharide (LPS) and incubated overnight (approximately 12 hours). In order to test the effect of CD44 blocking on the uptake of IR780-loaded micelles, after the overnight incubation, the medium was supplemented with 10 mg mL^{-1} HA for three hours to make sure the CD44 receptor on the cells is inhibited. The medium in the control chambers was replaced with fresh medium with 100 ng/ml LPS during this step. After the incubation with HA, the cells were washed with PBS ×3. IR780 loaded ITMs were added and incubated for 6 h. After incubation, the medium was removed and the cells were washed thrice with 1× DPBS, fixed with 4% paraformaldehyde (PFA), and counter-stained with 4′,6-diamidino-2-phenylindole (DAPI). The fluorescence was then visualized using microscopy (EVOS M7000 microscope, Thermo Fisher Scientific, MA, USA).

4.2.8. Cytokine analysis and luciferase reporter assay *in vitro*. To assess cytokine levels in the cell supernatant, LPS-treated cells (both cell types) at a density of 5 × 10^5 cells per mL were incubated in media containing 100 μM concentrations of both free RU.521 and RU.521 loaded in ITMs and subsequently incubated overnight. Following the incubation period, the cell supernatant was collected, and the concentrations of secreted cytokines were quantified utilizing a multi-bead-based assay with the Bio-Plex Pro™ system from Bio-Rad (Hercules, CA). To measure the activated NF-κB concentration, a semi-quantitative ELISA assay was used from Abcam (ab176663). 2 × 10^5 cells were incubated in an 8 well plate either in 500 μL culture medium or in medium supplemented with 100 ng ml^{-1} LPS to activate the inflammatory response. After overnight incubation, cells that were incubated in LPS containing medium received either 100 μM free RU.521 or the same amount of RU.521 loaded in ITMs, or none (to be assessed as the positive control; LPS only). After a 6-hour incubation period, the cells were lysed, and ELISA steps were completed following the kit manufacturer's instructions.

RAW 264.7 cGAS-knockout macrophages (RAW KO-cGAS) were cultured as per the manufacturer's instructions (InvivoGen, San Diego, CA, USA). The reporter assay was performed as per the manufacturer's instructions. Briefly, to activate the STING pathway, 10 μM cGAMP was added to the cells and subsequently treated with 50 μM and 100 μM concentrations of both free RU.521 and RU.521 loaded in micelles and subsequently incubated for 24 hours. After 24 h of incubation, the QUANTI-Luc™ 4 reagent was added, and luminescence was recorded using a multi-plate reader (SpectraMax iD3, Molecular Devices, San Jose, CA, USA).

4.2.9. ROS detection *in vitro*. Cellular ROS was detected *in vitro* by using DCFDA fluorescence. 2 × 10^5 cells were seeded in an 8 well plate either in 500 μL culture medium or in medium supplemented with 100 ng ml^{-1} LPS to activate the inflammatory response. After overnight incubation, cells that were incubated in LPS containing medium received either 100 μM free RU.521 or the same amount of RU.521 loaded in

ITMs, or none (to be assessed as the positive control; LPS only). After a 6-hour incubation period, cells were washed with 37 °C HBSS buffer to remove serum, and then a working solution of DCFDA in serum free DMEM at a concentration of 10 mM was added to the cells. The cells were incubated with the DCFDA working solution in the dark at 37 °C for 30 minutes, and then the medium was removed and cells were washed with 1× HBSS and transferred back into fresh HBSS. Cells were then immediately imaged live under a fluorescence microscope. Quantification of fluorescence was done with ImageJ software.

4.2.10. Animals. Animal experiments were performed as per the institutional laws of Iowa State University on ASF IL-10 knockout mice. All animals were bred and maintained at Iowa State University facilities and housed under pathogen-free conditions in the animal facility at the Advanced Teaching and Research Building (ATRB) of Iowa State University. Mice were housed for up to a month and randomly assigned to experimental groups.

4.2.11. Microbial-induced model of colitis. 8- to 20-week-old ASF IL-10 KO mice were given 1×10^7 *Helicobacter bilis via* oral gavage. ITMs (equivalent of 0.025 μmoles of RU.521) were administered orally twice every day (morning and afternoon) after the initial colonization with *H. bilis*. Change in body weight was recorded every day. Once the untreated group reached 80% of their initial weight, all mice were euthanized, and their feces, caecum, entire colon and spleens were collected. The colon length and spleen weights were measured. The mAbs given to mice were all purchased from InvivomAb and included anti-mouse IL-6 (Cat. No. BE0046), mouse IgG2a isotype control (Cat. No. BE0085), and anti-mouse IL-12 p40 (Cat. No. BE0051). To simulate a moderate microbial-induced colitis model, mice were colonized with 5×10^8 *Escherichia coli* 1D *via* oral gavage. *E. coli* 1D is an AIEC strain originally isolated from a dog with IBD, which was obtained from Dr Kenny Simpson, College of Veterinary Medicine, Cornell University. Following colonization, their daily weights were recorded and dosing with ITMs started 3 weeks after the inoculation date. Mice were given one dose of 0.025 μmoles of RU.521 loaded in ITMs daily for 20 days. Between days 34 and 38, their water was substituted with 2% DSS to trigger moderate colitis; afterwards the mice received normal water for two days and were euthanized on day 40. The disease activity index was estimated on the last day of the experiment by scoring weight loss (no weight loss: 1; 5–10% weight loss: 2; 11–15% weight loss: 3; 16–20% weight loss: 4; >20% weight loss: 5), stool consistency (formed: 1; soft: 2; very soft: 3; watery stool: 4), the degree of rectal bleeding (normal color stool: 1; brown color stool: 2; reddish color stool: 3; bloody stool: 4), and mobility of the mice (healthy and mobile: 1; ruffled fur: 2; slightly lethargic: 3; lethargic: 4; not mobile: 5).

Fecal lipocalin was measured on fresh fecal samples using the mouse lipocalin-2/NGAL ELISA kit from Biotechne (Cat. No. DY1857-05), according to the manufacturer's instructions. Fecal colony forming units (CFU) were calculated on the fecal matter of mice in the *E. coli* experiment. A homogenized solution of fecal matter in PBS was made with 1 : 10 weight : volume ratio. The solution was thoroughly mixed and made into a series of 7 serial dilutions, each diluted by a factor of 10. Three 10 μL aliquots of each dilution were placed on a section of a MacConkey agar plate and incubated at 37 °C for 24 h. After 24 h, the number of colonies in each section were counted and used to calculate the CFU per gram of fecal matter.

4.2.12. *In vivo* biodistribution. To evaluate the ability of ITMs to target the inflamed colon, seven days after the infection with *H. bilis*, 10 μg of IR780 loaded in ITMs solubilized in 250 μl of PBS (the equivalent of 0.5 mg kg^{-1} of IR780) was administered orally to each mouse. Mice were euthanized at two time points, 24 h and 48 h, and organs including kidney, lung, spleen, liver, stomach, caecum, colon, and intestine were excised and saved in both OCT and 10% formalin buffer. OCT tissues were sectioned at 8 μm thickness and then stained separately with CD44 and also F4/80, EpCAM, and DAPI and imaged under a revolving fluorescence microscope, with an unstained tissue acting as a fluorescent baseline.

4.2.13. Cytokine analysis and MPO activity in tissues *ex vivo*. Triplicate one-centimeter colon tissue pieces were harvested from each experimental mouse during necropsy, followed by a gentle wash in PBS and explant wash media. The tissue samples were then incubated at 37 °C for 24 h in colonic explant media. Afterwards, the supernatant was collected and frozen at −20 °C until further analysis. The secreted cytokine concentrations were estimated through a multi-bead-based assay from Bio-Plex Pro™ (Bio-Rad, Hercules, CA). Myeloperoxidase (MPO) activity was measured using the Abcam mouse MPO ELISA kit (ab285307). During necropsy, a 1 cm piece from distal colon was placed in homogenizer tubes and processed according to the manufacturer's protocol. All biological assay results were normalized to total protein with ThermoFisher's Pierce™ BCA protein assay kit (Cat. No. 23225). IFN-α ELISA was performed on mouse serum using ThermoFisher's Mouse IFN-alpha/beta R2 ELISA kit (REF: EM39RB).

4.2.14. Histopathology of tissues. The entire colon from the mouse was rolled into Swiss rolls, fixed in 10% buffered formalin, embedded in paraffin, and stained with hematoxylin and eosin (H&E). Microscopic changes and severity of histological damage were scored in a blinded manner by a board certified anatomic veterinary pathologist to avoid observer bias. Tissue damage, lamina propria inflammatory cell infiltration, inflammation severity, edema, and crypt changes were all assessed. Tissue damage was reviewed as follows: 0, none; 1, isolated focal epithelial damage, mostly limited to surface epithelium; 2, mucosal erosions and ulcerations; 3, extensive damage to the lamina propria, submucosa, and muscularis. The extent of inflammation was scored as follows: 0, none to superficial; 1, aggregates in the lamina propria only; 2, aggregates in the lamina propria and submucosa; 3, transmural cell aggregates. The severity of the inflammatory cell infiltration was the sum of the scores of the mucosa, submucosa and muscularis/serosa (up to 9 possible points). The inflammation severity was graded as 0, normal; 1, mild; 2, modest; 3, severe. Epithelial changes were scored as follows: 0, normal; 1, hyperplasia of crypt epithelium and goblet cell loss; 2, mild to

moderate crypt loss (5 to <50%); 3, severe crypt loss (50–90%); 4, complete crypt loss with retention of surface epithelium; 5, small- to medium-sized ulcers (<10 crypt widths); 6, large ulcers (≥10 crypt widths). Lastly, edema was scored as follows: 0, normal; 1, mild; 2, moderate; 3, severe. The scores for all parameters were summed for each animal to get a total histologic score (THS). A total score of 24 points was possible for each tissue sample evaluated following summation of histopathological parameter scores. The total histological scores (THSs) were then averaged per group for comparison of the means. The THSs were interpreted as follows: score 0, not affected; score 1–5, mild severity; score 6–10, mild to moderate severity; score 11–15, moderate severity; score 16–20, moderate to severe severity; score 21–24, severe severity.

4.2.15. Immunofluorescence in tissues. Immunofluorescence analysis for the biodistribution of ITMs (Fig. 4(a) and (b)) was done on OCT-frozen tissues and the remaining immunofluorescence experiments (Fig. 7(a)–(d) and Fig. S7a) were carried out using formalin-fixed, paraffin-embedded colonic tissue, prepared as Swiss rolls. Paraffin-embedded colonic sections were routinely processed and affixed to slides. Then antigen retrieval was performed by incubating slides in 95–100 °C citrate buffer for 10 minutes followed by blocking in 5% BSA in PBS and an optional permeabilization step of 10 minute incubation in 0.2% Triton-X. Anti-mouse F4/80 was purchased from Invitrogen (REF: MF48020, Lot: 2426542) and diluted 1 : 50, anti-mouse CD326 (EpCAM) was purchased from Invitrogen (REF: 17-5791-82, Lot: 2869669) and diluted 1 : 80, and anti-mouse ZO-1 was purchased from Proteintech (Cat. No. CL488-21773) and diluted 1 : 80. STING/TMEM173 primary antibody was purchased from Fischer Scientific (Cat. No. NBP224683) and diluted 1 : 100, and Alexa-fluor 680 goat anti-rabbit IgG (Cat. No. A21076) was purchased from Invitrogen and used as the secondary antibody at a dilution of 10 μg ml^{-1}. 4-HNE primary antibody was purchased from ThermoFisher (Cat. No. MA5-27570) and diluted 1 : 100, and goat anti-mouse Alexa fluor 488 was purchased from ThermoFisher (Cat. No. A-11001) and was used as the secondary antibody diluted 1 : 500. CD44 monoclonal antibody was purchased from ThermoFisher (Cat. No. 14-0441-82) and diluted 1 : 250, and FITC goat anti-rat IgG was purchased from Biolegend (Cat. No. 405404) and used as the secondary antibody diluted 1 : 500. ProLong™ Gold antifade reagent with DAPI was purchased from Invitrogen (REF: P36935). The Vector True View Autofluorescence Quenching kit (REF: SP-8400) was used to reduce background autofluorescence. OCT-frozen tissues were sectioned, fixed with MeOH, and washed 3 times with PBS to remove the remaining OCT. Afterwards the slides were blocked with 5% BSA in PBS for 10 minutes, and then incubated with the corresponding mixture of antibodies overnight at 4 °C. Slides were washed with PBS the next day and fixed with a DAPI mounting medium. ImageJ software was used to quantify the fluorescence by determining the mean brightness in every image. Three biological replicates were used for the quantification of each group.

4.2.16. Statistical analysis. All data are expressed as the mean ± standard deviation (S.D.). Statistical significance was determined using a two-tailed heteroscedastic Student's *t*-test and defined as $*p < 0.05$ $**p < 0.01$ and $***p < 0.001$, and n.s. indicates not significant.

Ethical statement

All animal procedures were performed in accordance with the Guidelines for Care and Use of Laboratory Animals of Iowa State University and approved by the Animal Ethics Committee of Institutional Animal Care and Use Committee (IACUC) under protocol number IACUC-21-194.

Author contributions

S. G. performed the polymer synthesis, carried out *in vitro* and *in vivo* experiments, and wrote the manuscript. S. H. assisted with the *in vivo* experiments and reviewed the manuscript. S.U. designed the polymer and trained on micelle synthesis. T. H. provided the histopathology images and the scoring. M. J. W. provided guidance and training in the *in vivo* studies, bred and provided the ASF IL-10KO mice, and edited the manuscript. R. B. conceived the project idea, directed the study design, provided guidance throughout the study, and edited the manuscript.

Conflicts of interest

The authors declare no conflict of interest.

Data availability

The data supporting this study's findings will be made available on DataShare, ISU's open access data repository.

Supporting information: Taxonomy of the bacterial species in ASF mice, schematic showing the chemical structure of the ITMs, additional FTIR, H-NMR and UV-vis characterization of the ITMs, comparison of NF-kB expression between MODE-k and J774.A1 cells, comparison of the different effects of low doses of DSS on ASF IL-10 KO mice, the plots of the normalized daily weights of the mid anti-IL-12p40 groups, the breakdown of each histopathology criterion such as tissue damage, inflammation severity in lamina propria, extent of inflammatory infiltrate, edema and crypt change, H&E images of the ITM + anti-IL-6 group, ITM+ IgG isotype group, mid anti-IL-12p40 group and ITM+ mid anti-IL-12p40 group. See DOI: https://doi.org/10.1039/d5nh00317b.

Acknowledgements

S. G. acknowledges support from the congressionally directed medical research program (CDMRP) award HT9425-23-1-0071. S. U. acknowledges support from the National Science Foundation award CMMI-2223689. R. B. acknowledges support from the Jean H. Steffenson Chair, CDMRP award HT9425-23-1-0071, and NSF award CMMI-2223689. M. J. W. acknowledges partial support from the DOD-Defense Threat Reduction Agency (DTRA) award HDTRA12110015.

References

1 B. A. Hendrickson, R. Gokhale and J. H. Cho, Clinical Aspects and Pathophysiology of Inflammatory Bowel Disease, *Clin. Microbiol. Rev.*, 2002, **15**, 79–94, DOI: **10.1128/CMR.15.1.79-94.2002**.

2 L. M. Keubler, M. Buettner, C. Häger and A. Bleich, A Multihit Model: Colitis Lessons from the Interleukin-10–deficient Mouse, *Inflammatory Bowel Dis.*, 2015, **21**, 1967–1975, DOI: **10.1097/MIB.0000000000000468**.

3 M. Saleh and G. Trinchieri, Innate immune mechanisms of colitis and colitis-associated colorectal cancer, *Nat. Rev. Immunol.*, 2011, **11**, 9–20, DOI: **10.1038/nri2891**.

4 A. Ablasser and Z. J. Chen, cGAS in action: Expanding roles in immunity and inflammation, *Science*, 2019, **363**, eaat8657, DOI: **10.1126/science.aat8657**.

5 A. Decout, J. D. Katz, S. Venkatraman and A. Ablasser, The cGAS–STING pathway as a therapeutic target in inflammatory diseases, *Nat. Rev. Immunol.*, 2021, **21**, 548–569, DOI: **10.1038/s41577-021-00524-z**.

6 G. R. Martin, C. M. Blomquist, K. L. Henare and F. R. Jirik, Stimulator of interferon genes (STING) activation exacerbates experimental colitis in mice, *Sci. Rep.*, 2019, **9**, 14281, DOI: **10.1038/s41598-019-50656-5**.

7 S. Khan, E. Novak, H. Mentrup, S. R. Ballesteros and K. Patrick Mollen, Activation of Cyclic GMP-AMP Synthase in Intestinal Epithelial Cells Contributes to Protection Against Colitis, *J. Am. Coll. Surg.*, 2020, **231**, S51, DOI: **10.1016/j.jamcollsurg.2020.07.080**.

8 L. Shmuel-Galia, F. Humphries, X. Lei, S. Ceglia, R. Wilson, Z. Jiang, N. Ketelut-Carneiro, S. E. Foley, S. Pechhold, J. Houghton, K. Muneeruddin, S. A. Shaffer, B. A. McCormick, A. Reboldi, D. Ward, A. Marshak-Rothstein and K. A. Fitzgerald, Dysbiosis exacerbates colitis by promoting ubiquitination and accumulation of the innate immune adaptor STING in myeloid cells, *Immunity*, 2021, **54**, 1137–1153, DOI: **10.1016/j.immuni.2021.05.008**.

9 S. Skopelja-Gardner, J. An and K. B. Elkon, Role of the cGAS–STING pathway in systemic and organ-specific diseases, *Nat. Rev. Nephrol.*, 2022, **18**, 558–572, DOI: **10.1038/s41581-022-00589-6**.

10 Q. Hu, H. Ren, G. Li, D. Wang, Q. Zhou, J. Wu, J. Zheng, J. Huang, D. A. Slade, X. Wu and J. Ren, STING-mediated intestinal barrier dysfunction contributes to lethal sepsis, *EBioMedicine*, 2019, **41**, 497–508, DOI: **10.1016/j.ebiom.2019.02.055**.

11 L. E. Pastora, N. S. Namburu, K. Arora, P. P. Christov and J. T. Wilson, STING-Pathway Inhibiting Nanoparticles (SPINs) as a Platform for Treatment of Inflammatory Diseases, *ACS Appl. Bio Mater.*, 2024, **7**, 4867–4878, DOI: **10.1021/acsabm.3c01305**.

12 J. Revés, R. C. Ungaro and J. Torres, Unmet needs in inflammatory bowel disease, *Curr. Res. Pharmacol. Drug Discov.*, 2021, **2**, 100070, DOI: **10.1016/j.crphar.2021.100070**.

13 C. Zhao, J. Yang, M. Chen, W. Chen, X. Yang, H. Ye, L. Wang, Y. Wang, J. Shi, F. Yue and X. Ma, Synthetic Lignin-Derived Therapeutic Nano Reagent as Intestinal pH-Sensitive Drug Carriers Capable of Bypassing the Gastric Acid Environment for Colitis Treatment, *ACS Nano*, 2023, **17**, 811–824, DOI: **10.1021/acsnano.2c11188**.

14 C. Oh, W. Lee, J. Park, J. Choi, S. Lee, S. Li, H. N. Jung, J.-S. Lee, J.-E. Hwang, J. Park, M. Kim, S. Baek and H.-J. Im, Development of Spleen Targeting H_2S Donor Loaded Liposome for the Effective Systemic Immunomodulation and Treatment of Inflammatory Bowel Disease, *ACS Nano*, 2023, **17**, 4327–4345, DOI: **10.1021/acsnano.2c08898**.

15 Y. Lee, K. Sugihara, M. G. Gillilland, S. Jon, N. Kamada and J. J. Moon, Hyaluronic acid–bilirubin nanomedicine for targeted modulation of dysregulated intestinal barrier, microbiome and immune responses in colitis, *Nat. Mater.*, 2020, **19**, 118–126, DOI: **10.1038/s41563-019-0462-9**.

16 W. Hao, R. Cha, M. Wang, P. Zhang and X. Jiang, Impact of nanomaterials on the intestinal mucosal barrier and its application in treating intestinal diseases, *Nanoscale Horiz.*, 2022, **7**, 6–30, DOI: **10.1039/D1NH00315A**.

17 S. Misra, V. C. Hascall, R. R. Markwald and S. Ghatak, Interactions between Hyaluronan and Its Receptors (CD44, RHAMM) Regulate the Activities of Inflammation and Cancer, *Front. Immunol.*, 2015, **6**, 201, DOI: **10.3389/fimmu.2015.00201**.

18 B. M. Wittig, R. Sabat, P. Holzlöhner, E. Witte-Händel, K. Heilmann, K. Witte, J. Triebus, A. Tzankov, J. D. Laman, B. Bokemeyer, L. Terracciano, C. Schwärzler, H. Kohler, R. Volkmer, C. Loddenkemper, K. Wolk, U. Hoffmann and U. Günthert, Absence of specific alternatively spliced exon of CD44 in macrophages prevents colitis, *Mucosal Immunol.*, 2018, **11**, 846–860, DOI: **10.1038/mi.2017.98**.

19 T. Xiong, H. Xu, Q. Nie, B. Jia, H. Bao, H. Zhang, J. Li, Z. Cao, S. Wang, L. Wu and J. Zhang, Reactive Oxygen Species Triggered Cleavage of Thioketal-Containing Supramolecular Nanoparticles for Inflammation-Targeted Oral Therapy in Ulcerative Colitis, *Adv. Funct. Mater.*, 2025, **35**, 2411979, DOI: **10.1002/adfm.202411979**.

20 S. Vasvani, A. Vasukutty, R. Bardhan, I.-K. Park and S. Uthaman, Reactive oxygen species driven prodrug-based nanoscale carriers for transformative therapies, *Biomater. Sci.*, 2024, **12**, 4335–4353, DOI: **10.1039/D4BM00647J**.

21 X. Ling, S. Zhang, P. Shao, P. Wang, X. Ma and M. Bai, Synthesis of a reactive oxygen species responsive heterobifunctional thioketal linker, *Tetrahedron Lett.*, 2015, **56**, 5242–5244, DOI: **10.1016/j.tetlet.2015.07.059**.

22 S. Uthaman, S. Parvinroo, A. P. Mathew, X. Jia, B. Hernandez, A. Proctor, K. A. Sajeevan, A. Nenninger, M.-J. Long, I.-K. Park, R. Chowdhury, G. J. Phillips, M. J. Wannemuehler and R. Bardhan, Inhibiting the cGAS-STING Pathway in Ulcerative Colitis with Programmable Micelles, *ACS Nano*, 2024, **18**, 12117–12133, DOI: **10.1021/acsnano.3c11257**.

23 C. Ma, D. Yang, B. Wang, C. Wu, Y. Wu, S. Li, X. Liu, K. Lassen, L. Dai and S. Yang, Gasdermin D in macrophages restrains colitis by controlling cGAS-mediated inflammation, *Sci. Adv.*, 2020, **6**, eaaz6717, DOI: **10.1126/sciadv.aaz6717**.

24 C. Yang and D. Merlin, Unveiling Colitis: A Journey through the Dextran Sodium Sulfate-induced Model, *Inflammatory Bowel Dis.*, 2024, **30**, 844–853, DOI: 10.1093/ibd/izad312.

25 A. Proctor, S. Parvinroo, T. Richie, X. Jia, S. T. M. Lee, P. D. Karp, S. Paley, A. D. Kostic, J. F. Pierre, M. J. Wannemuehler and G. J. Phillips, Resources to Facilitate Use of the Altered Schaedler Flora (ASF) Mouse Model to Study Microbiome Function, *mSystems*, 2022, **7**, e00293-22, DOI: 10.1128/msystems.00293-22.

26 M. Wymore Brand, M. J. Wannemuehler, G. J. Phillips, A. Proctor, A.-M. Overstreet, A. E. Jergens, R. P. Orcutt and J. G. Fox, The Altered Schaedler Flora: Continued Applications of a Defined Murine Microbial Community, *ILAR J.*, 2015, **56**, 169–178, DOI: 10.1093/ilar/ilv012.

27 M. B. Biggs, G. L. Medlock, T. J. Moutinho, H. J. Lees, J. R. Swann, G. L. Kolling and J. A. Papin, Systems-level metabolism of the altered Schaedler flora, a complete gut microbiota, *ISME J.*, 2017, **11**, 426–438, DOI: 10.1038/ismej.2016.130.

28 A.-M. C. Overstreet, A. E. Ramer-Tait, J. S. Suchodolski, J. M. Hostetter, C. Wang, A. E. Jergens, G. J. Phillips and M. J. Wannemuehler, Temporal Dynamics of Chronic Inflammation on the Cecal Microbiota in IL-10-/- Mice, *Front. Immunol.*, 2021, **11**, 585431, DOI: 10.3389/fimmu.2020.585431.

29 M. Liu, W. Yuan and S. Park, Association between IL-10 rs3024505 and susceptibility to inflammatory bowel disease: A systematic review and meta-analysis, *Cytokine*, 2022, **149**, 155721, DOI: 10.1016/j.cyto.2021.155721.

30 K. Engelhardt and B. Grimbacher, IL-10 in Humans: Lessons from the Gut, IL-10/IL-10 Receptor Deficiencies, and IL-10 Polymorphisms, *Interleukin-10 in Health and Disease*, Current Topics in Microbiology and Immunology, Springer, Berlin Heidelberg, 2014, pp. 1–18, DOI: 10.1007/978-3-662-43492-5_1.

31 L. Maggio-Price, D. Shows, K. Waggie, A. Burich, W. Zeng, S. Escobar, P. Morrissey and J. L. Viney, Helicobacter bilis Infection Accelerates and H. hepaticus Infection Delays the Development of Colitis in Multiple Drug Resistance-Deficient (mdr1a−/−) Mice, *Am. J. Pathol.*, 2002, **160**, 739–751, DOI: 10.1016/S0002-9440(10)64894-8.

32 T. Atherly, C. Mosher, C. Wang, J. Hostetter, A. Proctor, M. W. Brand, G. J. Phillips, M. Wannemuehler and A. E. Jergens, Helicobacter bilis Infection Alters Mucosal Bacteria and Modulates Colitis Development in Defined Microbiota Mice, *Inflammatory Bowel Dis.*, 2016, **22**, 2571–2581, DOI: 10.1097/MIB.0000000000000944.

33 Z. Liu, A. L. Henderson, D. Nettleton, J. H. Wilson-Welder, J. M. Hostetter, A. Ramer-Tait, A. E. Jergens and M. J. Wannemuehler, Mucosal gene expression profiles following the colonization of immunocompetent defined-flora C3H mice with Helicobacter bilis: a prelude to typhlocolitis, *Microbes Infect.*, 2009, **11**, 374–383, DOI: 10.1016/j.micinf.2008.12.013.

34 Z. R. Stromberg, A. Van Goor, G. A. J. Redweik, M. J. Wymore Brand, M. J. Wannemuehler and M. Mellata, Pathogenic and non-pathogenic *Escherichia coli* colonization and host inflammatory response in a defined microbiota mouse model, *Dis. Models Mech.*, 2018, **11**, dmm035063, DOI: 10.1242/dmm.035063.

35 P. Wetwittayakhlang and P. L. Lakatos, Advanced combination therapy: is it the best way to break the therapeutic ceiling, *Ther. Adv. Gastroenterol.*, 2024, **17**, 17562848241272995, DOI: 10.1177/17562848241272995.

36 J. K. Triantafillidis, C. G. Zografos, M. M. Konstadoulakis and A. E. Papalois, Combination treatment of inflammatory bowel disease: Present status and future perspectives, *World J. Gastroenterol.*, 2024, **30**, 2068–2080, DOI: 10.3748/wjg.v30.i15.2068.

37 J. Lesley, R. Hyman, N. English, J. B. Catterall and G. A. Turner, CD44 in inflammation and metastasis, *Glycoconj. J.*, 1997, **14**, 611–622, DOI: 10.1023/A:1018540610858.

38 E. Puré and C. A. Cuff, A crucial role for CD44 in inflammation, *Trends Mol. Med.*, 2001, **7**, 213–221, DOI: 10.1016/S1471-4914(01)01963-3.

39 P. Johnson and B. Ruffell, CD44 and its Role in Inflammation and Inflammatory Diseases, *Inflamm. Allergy – Drug Targets*, 2009, **8**, 208–220, DOI: 10.2174/187152809788680994.

40 T. Liu, L. Zhang, D. Joo and S.-C. Sun, NF-κB signaling in inflammation, *Signal Transduct. Target. Ther.*, 2017, **2**, 17023, DOI: 10.1038/sigtrans.2017.23.

41 F. D'Acquisto, F. De Cristofaro, M. C. Maiuri, G. Tajana and R. Carnuccio, Protective role of nuclear factor kappa B against nitric oxide-induced apoptosis in J774 macrophages, *Cell Death Differ.*, 2001, **8**, 144–151, DOI: 10.1038/sj.cdd.4400784.

42 Y. H. Park, N. Kim, Y. K. Shim, Y. J. Choi, R. H. Nam, Y. J. Choi, M. H. Ham, J. H. Suh, S. M. Lee, C. M. Lee, H. Yoon, H. S. Lee and D. H. Lee, Adequate Dextran Sodium Sulfate-induced Colitis Model in Mice and Effective Outcome Measurement Method, *J. Cancer Prev.*, 2015, **20**, 260–267, DOI: 10.15430/JCP.2015.20.4.260.

43 B. Chassaing, G. Srinivasan, M. A. Delgado, A. N. Young, A. T. Gewirtz and M. Vijay-Kumar, Fecal Lipocalin 2, a Sensitive and Broadly Dynamic Non-Invasive Biomarker for Intestinal Inflammation, *PLoS One*, 2012, **7**, e44328, DOI: 10.1371/journal.pone.0044328.

44 R. Wang, S. Cao, M. E. H. Bashir, L. A. Hesser, Y. Su, S. M. C. Hong, A. Thompson, E. Culleen, M. Sabados, N. P. Dylla, E. Campbell, R. Bao, E. B. Nonnecke, C. L. Bevins, D. S. Wilson, J. A. Hubbell and C. R. Nagler, Treatment of peanut allergy and colitis in mice via the intestinal release of butyrate from polymeric micelles, *Nat. Biomed. Eng.*, 2022, **7**, 38–55, DOI: 10.1038/s41551-022-00972-5.

45 M. K. Jeengar, D. Thummuri, M. Magnusson, V. G. M. Naidu and S. Uppugunduri, Uridine Ameliorates Dextran Sulfate Sodium (DSS)-Induced Colitis in Mice, *Sci. Rep.*, 2017, **7**, 3924, DOI: 10.1038/s41598-017-04041-9.

46 G. R. Lichtenstein, M. A. Kamm, P. Boddu, N. Gubergrits, A. Lyne, T. Butler, K. Lees, R. E. Joseph and W. J. Sandborn, Effect of Once- or Twice-Daily MMX Mesalamine (SPD476)

for the Induction of Remission of Mild to Moderately Active Ulcerative Colitis, *Clin. Gastroenterol. Hepatol.*, 2007, **5**, 95–102, DOI: 10.1016/j.cgh.2006.10.025.

47 M. Naganuma, N. Aoyama, Y. Suzuki, H. Nishino, K. Kobayashi, F. Hirai, K. Watanabe and T. Hibi, Twice-daily Budesonide 2-mg Foam Induces Complete Mucosal Healing in Patients with Distal Ulcerative Colitis, *J. Crohns Colitis*, 2016, **10**, 828–836, DOI: 10.1093/ecco-jcc/jjv208.

48 H. Kittana, J. C. Gomes-Neto, K. Heck, A. L. Geis, R. R. Segura Muñoz, L. A. Cody, R. J. Schmaltz, L. B. Bindels, R. Sinha, J. M. Hostetter, A. K. Benson and A. E. Ramer-Tait, Commensal Escherichia coli Strains Can Promote Intestinal Inflammation via Differential Interleukin-6 Production, *Front. Immunol.*, 2018, **9**, 2318, DOI: 10.3389/fimmu.2018.02318.

49 R. B. Holmstroem, O. H. Nielsen, S. Jacobsen, L. B. Riis, S. Theile, J. T. Bjerrum, P. Vilmann, J. S. Johansen, M. K. Boisen, R. H. L. Eefsen, I. Marie Svane, D. L. Nielsen and I. M. Chen, COLAR: open-label clinical study of IL-6 blockade with tocilizumab for the treatment of immune checkpoint inhibitor-induced colitis and arthritis, *J. Immunother. Cancer*, 2022, **10**, e005111, DOI: 10.1136/jitc-2022-005111.

50 K. Kawashima, M. Onizawa, T. Fujiwara, N. Gunji, H. Imamura, K. Katakura and H. Ohira, Evaluation of the relationship between the spleen volume and the disease activity in ulcerative colitis and Crohn disease, *Medicine*, 2022, **101**, e28515, DOI: 10.1097/MD.0000000000028515.

51 B. Chami, N. J. J. Martin, J. M. Dennis and P. K. Witting, Myeloperoxidase in the inflamed colon: A novel target for treating inflammatory bowel disease, *Arch. Biochem. Biophys.*, 2018, **645**, 61–71, DOI: 10.1016/j.abb.2018.03.012.

52 M. F. Neurath, Cytokines in inflammatory bowel disease, *Nat. Rev. Immunol.*, 2014, **14**, 329–342, DOI: 10.1038/nri3661.

53 K. Mitsuyama, S. Matsumoto, J. Masuda, H. Yamasakii, K. Kuwaki, H. Takedatsu and M. Sata, Therapeutic strategies for targeting the IL-6/STAT3 cytokine signaling pathway in inflammatory bowel disease, *Anticancer Res.*, 2007, **27**, 3749–3756.

54 Y. Guo, B. Wang, T. Wang, L. Gao, Z. Yang, F. Wang, H. Shang, R. Hua and J. Xu, Biological characteristics of IL-6 and related intestinal diseases, *Int. J. Biol. Sci.*, 2021, **17**, 204–219, DOI: 10.7150/ijbs.51362.

55 J. Ahn, S. Son, S. C. Oliveira and G. N. Barber, STING-Dependent Signaling Underlies IL-10 Controlled Inflammatory Colitis, *Cell Rep.*, 2017, **21**, 3873–3884, DOI: 10.1016/j.celrep.2017.11.101.

56 D. Pugliese, G. Privitera, M. Fiorani, L. Parisio, V. Calvez, A. Papa, A. Gasbarrini and A. Armuzzi, Targeting IL12/23 in ulcerative colitis: update on the role of ustekinumab, *Ther. Adv. Gastroenterol.*, 2022, **15**, 17562848221102283, DOI: 10.1177/17562848221102283.

57 T. Ochsenkühn, C. Tillack, D. Szokodi, S. Janelidze and F. Schnitzler, Clinical outcomes with ustekinumab as rescue treatment in therapy-refractory or therapy-intolerant ulcerative colitis, *United Eur. Gastroenterol. J.*, 2020, **8**, 91–98, DOI: 10.1177/2050640619895361.

58 F. Rob, D. Schierova, Z. Stehlikova, J. Kreisinger, R. Roubalova, S. Coufal, M. Mihula, Z. Jackova, M. Kverka, T. Thon, K. Kostovcikova, L. Bajer, P. Drastich, J. T. Hercogova, M. Novakova, M. Kolar, M. Vasatko, M. Lukas, H. Tlaskalova-Hogenova and Z. Jiraskova Zakostelska, Association between ustekinumab therapy and changes in specific anti-microbial response, serum biomarkers, and microbiota composition in patients with IBD: A pilot study, *PLoS One*, 2022, **17**, e0277576, DOI: 10.1371/journal.pone.0277576.

59 J.-S. Zhang, W.-G. Feng, C.-L. Li, X.-Y. Wang and Z.-L. Chang, NF-κB Regulates the LPS-Induced Expression of Interleukin 12 p40 in Murine Peritoneal Macrophages: Roles of PKC, PKA, ERK, p38 MAPK, and Proteasome, *Cell. Immunol.*, 2000, **204**, 38–45, DOI: 10.1006/cimm.2000.1690.

60 B. Khor, A. Gardet and R. J. Xavier, Genetics and pathogenesis of inflammatory bowel disease, *Nature*, 2011, **474**, 307–317, DOI: 10.1038/nature10209.

61 L. Huang, Y. Yang, F. Yang, S. Liu, Z. Zhu, Z. Lei and J. Guo, Functions of EpCAM in physiological processes and diseases (Review), *Int. J. Mol. Med.*, 2018, **24**, 1771–1785, DOI: 10.3892/ijmm.2018.3764.

62 L. S. Poritz, K. I. Garver, C. Green, L. Fitzpatrick, F. Ruggiero and W. A. Koltun, Loss of the Tight Junction Protein ZO-1 in Dextran Sulfate Sodium Induced Colitis, *J. Surg. Res.*, 2007, **140**, 12–19, DOI: 10.1016/j.jss.2006.07.050.

63 Q.-W. Chen, M.-W. Cao, J.-Y. Qiao, Q.-R. Li and X.-Z. Zhang, Integrated cascade catalysis of microalgal bioenzyme and inorganic nanozyme for anti-inflammation therapy, *Nanoscale Horiz.*, 2023, **8**, 489–498, DOI: 10.1039/D2NH00572G.

64 S. Ibrahim, X. Zhu, X. Luo, Y. Feng and J. Wang, PIK3R3 regulates ZO-1 expression through the NF-kB pathway in inflammatory bowel disease, *Int. Immunopharmacol.*, 2020, **85**, 106610, DOI: 10.1016/j.intimp.2020.106610.